

# <sup>1</sup> A robust method for measuring <sup>2</sup> aminoacylation through tRNA-Seq

<sup>3</sup> Kristian Davidsen<sup>1,2</sup> and Lucas B Sullivan<sup>1\*</sup>

\*For correspondence:  
lucas@fredhutch.org (LBS)

<sup>4</sup> <sup>1</sup>Fred Hutchinson Cancer Center; <sup>2</sup>Molecular and cellular biology program, University of  
<sup>5</sup> Washington

<sup>6</sup> 

---

<sup>7</sup> **Abstract** tRNA aminoacylation levels are difficult to quantify with current methods having either  
<sup>8</sup> low throughput or low precision and/or accuracy. We present an optimized charge tRNA-Seq  
<sup>9</sup> method combining new and previously described developments to generate precise and accurate  
<sup>10</sup> tRNA charge measurements. We show several controls and tests for validation of quantitation and  
<sup>11</sup> provide an end-to-end method that scales to hundreds of samples including software for data  
<sup>12</sup> processing. Our method also supports using the charge tRNA-Seq data to determine relative  
<sup>13</sup> expression levels and reverse transcription misincorporations to infer RNA modifications.

<sup>14</sup> 

---

## <sup>15</sup> Introduction

<sup>16</sup> Quantification of transfer RNA (tRNA) aminoacylation levels, also referred to as charge, has been  
<sup>17</sup> performed using radiolabeling (*Wolfson and Uhlenbeck, 2002*), Northern blotting (*Ho and Kan,  
1987; Varshney et al., 1991; Stenum et al., 2017*), DNA microarrays (*Dittmar et al., 2005*) and  
<sup>19</sup> high-throughput sequencing (*Evans et al., 2017*). While radiolabeling is very accurate, it is lim-  
<sup>20</sup> ited to purified tRNAs undergoing lab manipulation. Northern blotting uses differential migration  
<sup>21</sup> of acylated tRNA during electrophoresis to measure acylation levels. However, this has many  
<sup>22</sup> known limitations such as cross-binding probes, low sensitivity, low throughput on multiple tR-  
<sup>23</sup> NAs, insufficient band separation etc. Chemical differentiation of acylated tRNAs combined with  
<sup>24</sup> DNA microarrays were introduced to circumvent the problems with Northern blotting, but were  
<sup>25</sup> superseded by high-throughput sequencing enabling quantification on all tRNAs in one experiment.

<sup>26</sup> Chemical differentiation of acylated tRNAs is achieved using the Malaprade reaction to attack  
<sup>27</sup> the 2,3-dihydroxyls on the 3' ribose of deacylated tRNA, causing ring opening and destabilization.  
<sup>28</sup> The destabilized base is then eliminated using high pH and heat. This sequence of reactions was  
<sup>29</sup> characterized and used extensively in the past in an effort to sequence RNA molecules (*Whitfeld  
30 and Markham, 1953; Whitfeld, 1954; Khym and Cohn, 1961; Neu and Heppel, 1964*), and while futile  
<sup>31</sup> for RNA sequencing, it has proven a highly useful method to "tag" deacylated tRNAs by introducing  
<sup>32</sup> a single base truncation. We shall refer to this sequence of reactions as the "Whitfeld reaction"  
<sup>33</sup> (*Figure 1—figure Supplement 1*).

<sup>34</sup> The accuracy and robustness of the aminoacylation measurement depends on two parts: the  
<sup>35</sup> completeness of the Whitfeld reaction and the quality of tRNA sequencing (tRNA-Seq). A major  
<sup>36</sup> problem in tRNA-Seq is base modifications known to be numerous on tRNAs. These can lead  
<sup>37</sup> to stalling, misincorporation, skipping or falloff during the reverse transcription (RT) step of the  
<sup>38</sup> sequencing protocol (*Motorin et al., 2007*). The RT polymerase is most severely affected by base  
<sup>39</sup> modifications disrupting the Watson-Crick base pairing, while other modifications are often less  
<sup>40</sup> affected or silent (*Wang et al., 2021; Sas-Chen and Schwartz, 2019*). To increase RT readthrough  
<sup>41</sup> the demethylase AlkB has been used (*Zheng et al., 2015; Cozen et al., 2015*), while more recently  
<sup>42</sup> optimization of incubation conditions, including low salt and extended incubation time, has shown

43 large increases in readthrough (*Behrens et al., 2021*). But other factors can lead to errors in tRNA-  
44 Seq such as low RNA integrity, incomplete deacylation prior to adapter ligation, adapter ligation  
45 bias, PCR amplification bias and problems in read alignment.

46 Adapter ligation bias is a well documented problem in small RNA sequencing (*Fuchs et al., 2015*;  
47 *Zhuang et al., 2012*), receiving little attention in most tRNA-Seq protocols where it is particularly  
48 problematic because adapters often incorporate a barcode for sample multiplexing. The problem  
49 is further exacerbated when tRNA-Seq is coupled with the Whitfeld reaction, because this creates  
50 different sequence contexts for aminoacylated and deacylated tRNAs. One solution is to optimize  
51 conditions such that the ligation goes to completion. To that end, the tRNA structure can be used  
52 as it contains four nucleotides on the 3' end not participating in the basepairing of the acceptor  
53 stem. These are the discriminator base followed by the invariant CCA-end (*Figure 1*). These free  
54 nucleotides can be engaged in basepairing by an oligo splint designed to guide the ligation of the  
55 adapter and this approach has shown high tRNA specificity and ligation efficiency *Shigematsu et al.*  
56 (*2017*); *Smith et al.* (*2015*).

57 Read mapping is another known problem for tRNA-Seq. It arises due to the high error-rate of the  
58 RT polymerase when reading through modified bases in addition to frequent falloff. In combination,  
59 reads will frequently not have any continuous stretch of more than 15 nt. that perfectly match its  
60 reference. This is a problem for almost all alignment algorithms because they rely on some variation  
61 of subsequence matching to enable speed-up. The problem has been addressed by clustering of  
62 the reference sequences (*Hoffmann et al., 2018*) as well as masking known modified positions in  
63 the reference sequences (*Behrens et al., 2021*).

64 In recent years many variations of the tRNA-Seq method have been published (*Wang et al., 2021*;  
65 *Zheng et al., 2015*; *Cozen et al., 2015*; *Shigematsu et al., 2017*; *Erber et al., 2020*; *Thomas et al., 2021*;  
66 *Lucas et al., 2023*; *Pinkard et al., 2020*; *Warren et al., 2021*; *Yamagami and Hori, 2022*), but only  
67 few couple it with the Whitfeld reaction to probe aminoacylation levels (*Evans et al., 2017*; *Behrens*  
68 *et al., 2021*; *Watkins et al., 2022*) and little is known about the precision and accuracy of these  
69 measurements. Here, we present an up-to-date method for charge tRNA-Seq that ingrates new and  
70 existing developments including improved Whitfeld reaction chemistry, splint assisted ligation, high  
71 readthrough RT-PCR and improved read mapping, enabling us to measure tRNA charge, expression  
72 and modifications (*Figure 1*). We perform tests of the quantitative capabilities of the method and  
73 quantify its precision and accuracy. Finally, we provide an open-source code repository, enabling  
74 users to try our read processing, mapping using non-heuristic alignment and statistical tools on  
75 their own data (<https://github.com/krdav/tRNA-charge-seq>).

## 76 Results

### 77 Optimizing the Whitfeld reaction for charge tRNA-Seq

78 The use of periodate oxidation to discriminate aminoacylated tRNA was first used by *Dittmar et al.*  
79 (*2005*) for microarray measurements and then elegantly adapted to high-throughput sequencing by  
80 *Evans et al. (2017)*. However, we found noticeable differences between the conditions reported  
81 optimal for periodate oxidation in biochemical assays in the past (*Khym and Cohn, 1961*; *Neu and*  
82 *Heppel, 1964*; *Khym and Uziel, 1968*; *Dyer, 1956*) and those used in charge tRNA-Seq today (*Evans*  
83 *et al., 2017*; *Behrens et al., 2021*; *Watkins et al., 2022*; *Pavlova et al., 2020*; *Tsukamoto et al., 2022*).  
84 We therefore reasoned that it would be valuable to find a set of optimal conditions for the Whitfeld  
85 reaction when applied to charge tRNA-Seq. To do this, we used an E.coli tRNA-Lys-CCA oligo and  
86 measured conversion to its 1 nt. truncated product.

87 Periodate oxidation of cis-glycols is known to occur rapidly, even at low temperature (*Dyer,*  
88 *1956*); therefore, we tested if oxidation could be performed on ice to protect tRNA aminoacylations  
89 prone to hydrolysis. We found that complete oxidation is achieve after just 5 min (*Figure 2*, panel A)  
90 and therefore chose 10 min as optimal, with incubation on ice and in the dark because sunlight  
91 induces periodate oxidation side-reactions (*Erskine et al., 1953*).

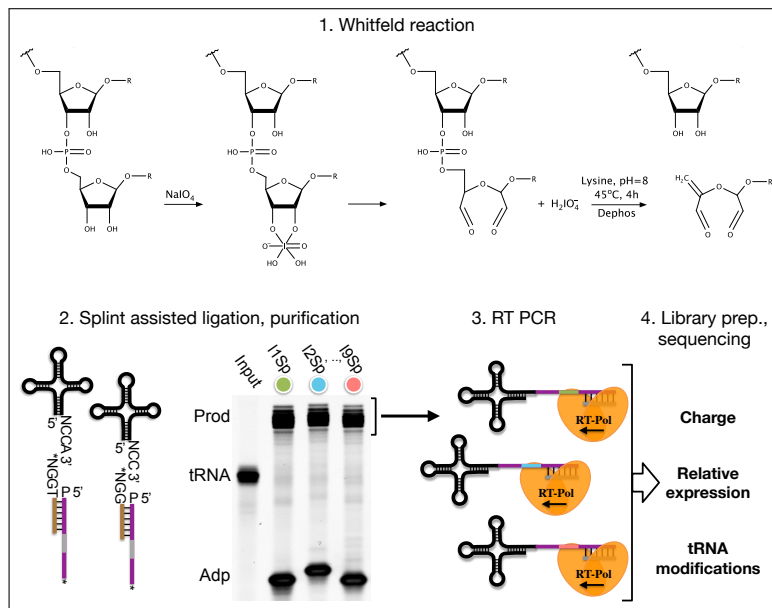


**Figure 1.** Summary illustrating the steps of the charge tRNA-Seq method we used to measure aminoacetylation, relative expression and tRNA modification levels. First, the Whitfeld reaction (detailed in *Figure 1—figure Supplement 1*) is used to discriminate between tRNAs with and without an aminoacetylation by cleaving off the 3' base of deacylated tRNA. Second, the tRNA is folded to expose the discriminator base (N) followed by the CCA/CC-end, creating a sticky-end for splint assisted ligation to a barcoded adapter. Stars (\*) on the 3' end of splint and adapter oligos indicate modifications to block self-ligation. Third, using the purified ligation product, RT-PCR is used to generate cDNA. Fourth, the cDNA is converted into a dsDNA library and sequenced to determine tRNA charge, expression and modifications.

**Figure 1—figure supplement 1.** Whitfeld reaction scheme.

Oxidation of deacylated tRNA yields a dialdehyde on the terminal ribose which enables the phosphoric ester linkage to be broken in a  $\beta$ -elimination reaction (*Rammler, 1971; Uziel, 1973*), yielding an unsaturated product (*Figure 1—figure Supplement 1*). While this cleavage reaction is complex, involving several semi-stable intermediates and different pathways depending on the pH, it appears to be induced by high pH and the presence of a primary amine (*Uziel, 1975*). Lysine has been identified as a good source of primary amine and incubation at 45°C has been found optimal (*Khym and Cohn, 1961; Neu and Heppel, 1964*). In previous charge tRNA-Seq methods, a borax buffered solution at pH=9.5 has been used to induce cleavage, instead we wanted to test using lysine at pH=8 to improve RNA stability. We found complete cleavage after 90 min (*Figure 2*, panel B); however, this step also serves as deacylation step and some aminoacylations were measurable after 90 min of lysine cleavage (*Figure 2—figure Supplement 1*, panel A). Therefore, we settled on a 4 h incubation time, but even with this extended incubation, the decrease in pH made a large improvement on RNA integrity (*Figure 2*, panel C).

Finally, we wanted to perform the Whitfeld reaction as a one-pot reaction as shown by *Watkins et al. (2022)*. However, we found that the typically quenchers used to remove unreacted periodate, glucose or ribose, are not compatible with lysine induced cleavage (*Figure 2—figure Supplement 1*, panel C). This is likely due to the generation of dialdehydes that cross-link lysines; therefore, we chose to use ethylene glycol which only forms formaldehyde upon periodate oxidation. Additionally, ethylene glycol reacts fast and can be added in high molar excess without negatively affecting subsequent steps, thus enabling the whole Whitfeld reaction in one tube (*Figure 2*, panel D).

### 112 Adapter ligation introduce charge measurement bias

113 Following the Whitfeld reaction tRNAs must be sequenced in order to measure aminoacetylation  
114 levels. To achieve this with enough throughout, we chose to ligate to barcoded adapters to enable

sample pooling before the RT-PCR step (*McGlincy and Ingolia, 2017*). We followed the protocol of *Behrens et al. (2021)*, with minor modifications to the oligo design, but found that the measured charge was highly variable between replicates and that the measurements were biased by the barcode identity to an unacceptable degree (*Figure 2—figure Supplement 2*). We hypothesized that this is due to ligation bias commonly encountered in blunt-end ligation (*Fuchs et al., 2015; Zhuang et al., 2012; Jayaprakash et al., 2011*) and reasoned that increasing ligation efficiency could mitigate the bias. However, our attempts to improved ligation efficiency failed as we were never able to reach more than ~50% ligation of the input tRNA (*Figure 2—figure Supplement 3*).

### 123 **Splint assisted ligation improves efficiency**

124 Inspired by *Smith et al. (2015)* and *Shigematsu et al. (2017)* we turned to splint assisted ligation.  
125 This approach utilizes that tRNAs have four nucleotides protruding from the 3' end and available for  
126 basepairing: the discriminator base, which can be any of the four RNA nucleotides, followed by the  
127 invariant CCA-end. The splint oligo is designed to bind both the 3' end of tRNAs and the 5' end of an  
128 adapter (*Figure 1*), thus bringing the two into proximity and increasing ligation efficiency. However,  
129 whereas earlier uses of splint assisted ligation could assume that all tRNAs end on CCA, we have a mix  
130 of CCA and CC-ending tRNAs and therefore needed to use two splints. As tRNAs compete for ligation  
131 it is imperative that CCA-ending tRNAs, with stronger interaction with the splint, is not favoured.  
132 Fortunately, we observed a near complete ligation between all of our nine barcoded adapters and  
133 both CCA-ending human tRNA and a CC-ending tRNA-Lys oligo (*Figure 2—figure Supplement 4*,  
134 panel A and B). The ligation was specific as it was fully dependent on complementarity between the  
135 tRNA and the splint (*Figure 2—figure Supplement 4*, panel C). As we are only interested in ligation  
136 between tRNA and adapter, we block all other possible ligations through dephosphorylation of  
137 the tRNA and oligo modifications blocking the 3' end of adapter and splint oligos. This affords us  
138 the advantage of using a pure DNA splint without any RNA nucleotides as those used in previous  
139 publications (*Smith et al., 2015; Shigematsu et al., 2017; Pinkard et al., 2020; Warren et al., 2021;*  
140 *Thomas et al., 2021; Lucas et al., 2023*).

141 Importantly, we validated that tRNA processed using the one-pot Whitfeld reaction could be  
142 effectively used as substrate in the ligation reaction (*Figure 2*, panel E). We noted that a small  
143 amount of unligated tRNA appeared in reactions with tRNA oxidized with periodate. This unligated  
144 tRNA is of unknown origin and largely refractory to further ligation (*Figure 2—figure Supplement 5*,  
145 panel B); however, as shown later using charge titration, this did not have a measurable impact on  
146 the accuracy of the aminoacylation measurement.

### 147 **Combining optimizations results in a robust method for measuring tRNA charge**

148 After combining the optimized Whitfeld reaction with subsequent splint assisted ligation, we used  
149 the RT-PCR method proposed by *Behrens et al. (2021)* using the TGIRT polymerase (*Mohr et al., 2013*)  
150 to maximize the readthrough of modified nucleotides. We later found that high readthrough also  
151 could be achieved using Maxima RT polymerase (*Figure 2—figure Supplement 7*). The RT-PCR was  
152 primed by an oligo containing a 10 nt. unique molecular identifier (UMI) to diversify the sequence  
153 context for the subsequent circular ligation and allow collapsing of PCR replicates during data  
154 analysis. A final PCR was performed to attach Illumina barcodes to pool samples for multiplex  
155 sequencing.

156 Using this as our final charge tRNA-Seq method, we use the E.coli tRNA-Lys-CCA oligo as a  
157 spike-in control before the Whitfeld reaction to validate near complete conversion to its CC-end,  
158 suggesting efficient periodate oxidation (*Figure 2—figure Supplement 6*, panel A). Similarly, we  
159 validated the completeness of deacylation using deacylated controls and the integrity of the tRNA  
160 CCA-end using non-oxidized controls (*Figure 2—figure Supplement 6*, panel B and C). We then  
161 measured the baseline charge of H1299 cells grown in DMEM using four replicates, observing  
162 excellent repeatability and high charge for most codons except tRNA<sup>Ser</sup> codons and a tRNA<sup>Glu</sup>  
163 codon, validating observation by *Evans et al. (2017)* (*Figure 2*, panel F).

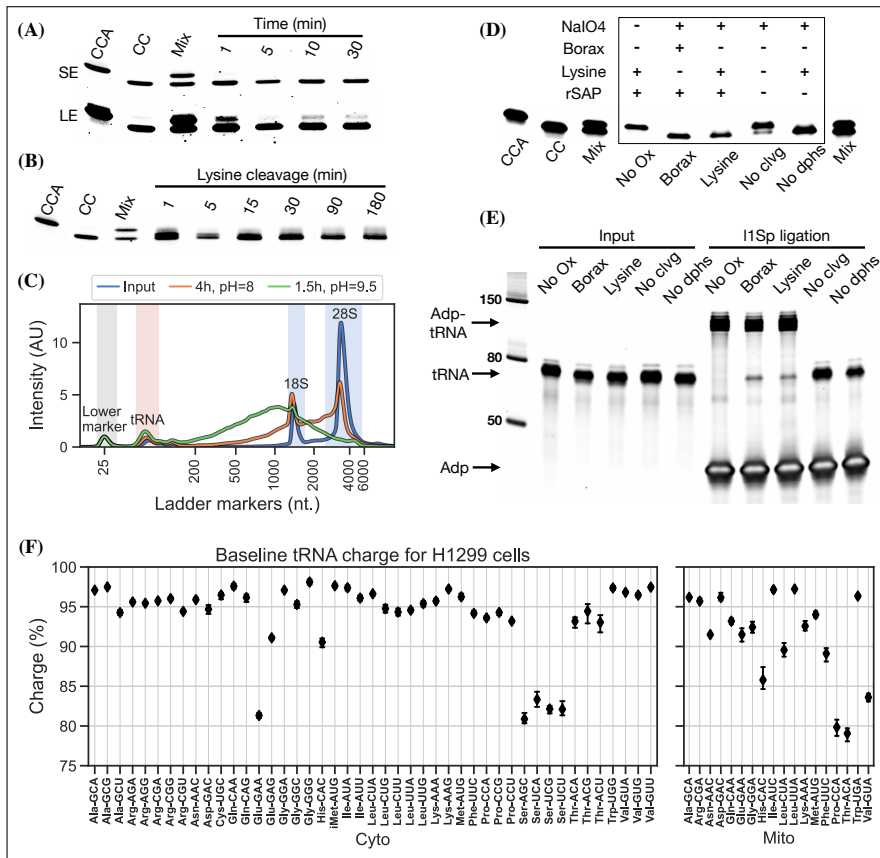


**Figure 2.** Optimizing the chemistry of charge tRNA-Seq. **(A)** Time required to complete periodate oxidation of the E.coli tRNA-Lys-CCA oligo on ice. Following oxidation, RNA was processed similar to *Evans et al. (2017)* to cleave off the 3' adenosine. Successful cleavage produce E.coli tRNA-Lys-CC. CCA, input oligo. CC, product oligo. Mix, 50/50 mix of CCA and CC. SE, short exposure. LE, long exposure. **(B)** Time required to complete lysine cleavage of the E.coli tRNA-Lys-CCA oligo (CCA) at 45°C, pH=8. Except the cleavage step, RNA was processed similar to *Evans et al. (2017)*. **(C)** TapeStation electropherogram comparing stability of whole cell RNA before and after 4 h lysine cleavage at pH=8 or 1.5 h borax cleavage at pH=9.5. tRNA range marked by red background, 18/28S by blue. See *Figure 2—figure Supplement 1*, panel B for RNA stability timecourse as it occurs on a gel. **(D)** Effect of individual components on cleavage of the E.coli tRNA-Lys-CCA oligo (CCA). All samples were processed as a one-pot reaction, except the borax sample which was processed similar to *Evans et al. (2017)*. rSAP, shrimp alkaline phosphatase. **(E)** Ligation test comparing the effect of RNA processing. Deacylated and gel purified human tRNA was processed identically as in panel (D), then ligated to l1Sp. Other adapters were tested with similar results (*Figure 2—figure Supplement 5*, panel A). **(F)** Baseline tRNA aminoacylation charge in H1299 cells grown in DMEM (4 replicates, bootstrapped 95% confidence interval of the mean). Charge on tRNA<sup>His</sup> is likely erroneously low because the discriminator base is shielded by base pairing (*Heinemann et al., 2012*), creating a steric hindrance for the splint assisted ligation.

**Figure 2—figure supplement 1.** Optimizing lysine induced cleavage.

**Figure 2—figure supplement 2.** Measurement bias in charge tRNA-Seq using blunt-end ligation.

**Figure 2—figure supplement 3.** tRNA-adapter blunt-end ligation attempted optimization.

**Figure 2—figure supplement 4.** Splint assisted ligation is highly efficient.

**Figure 2—figure supplement 5.** Ligation tests, related to panel E.

**Figure 2—figure supplement 6.** Sequenced controls.

**Figure 2—figure supplement 7.** RT readthrough comparing TGIRT to Maxima.

**Figure 2—figure supplement 8.** tRNA homology requires careful PCR conditions.

## Reference masking improves read mapping

It has previously been noted that alignment of tRNA reads is challenging due to RT misincorporations and falloff ([Hoffmann et al., 2018](#); [Behrens et al., 2021](#)). Most commonly, the Bowtie1 or Bowtie2

aligners have been applied using various settings to accommodate short reads and the many mismatches (*Cozen et al., 2015; Zheng et al., 2015; Clark et al., 2016; Evans et al., 2017; Pinkard et al., 2020*). However, although these are ultra-fast, Bowtie1 does not support alignments with insertions or deletions, and while Bowtie2 does, neither can guarantee that the best alignment is returned (*Langmead et al., 2009; Langmead and Salzberg, 2012*). We reasoned that many users of tRNA-Seq would rather sacrifice computational speed over mapping accuracy and therefore we apply a full all-against-all local alignment using the Smith-Waterman algorithm to provide the guaranteed best alignment(s). This is possible because the set of tRNA transcripts in a reference is only a few hundred sequences and thus we are able to align 1e8 tRNA-Seq reads to a human tRNA reference with 282 sequences in XXX h on a YYYY [number of cores, clock speed].

In addition to the choice of read alignment method, *Behrens et al. (2021)* found that using a SNP-tolerant alignment substantially improved mapping when modified positions were defined as SNPs. We adapted this approach by masking modified positions in the reference to "N"; however, we cannot rely on annotated modifications because these are incomplete and their effect on RT misincorporation rates is hard to predict. Instead, we used the misincorporation information embedded in the sequencing data, extracting it after a first pass alignment and then using mismatch frequencies for reference masking. As such, this is an iterative process because the alignment will change slightly with a new masked reference. In addition to the number of iterations, masking is only applied on positions with a minimum mismatch frequency (`min_mut_freq`) and either including or excluding reads with multiple transcript alignments (`unique_anno_float`). Furthermore, a parameter (`frac_max_score`) controls the sharing of a mask to highly similar transcripts. To find the optimal combination of parameters for reference masking we performed a grid search with the objective of finding the masking that resulted in the least number of reads assigned to transcripts with multiple codons (*Figure 3*, panel A). This lead to 334 positions in the 282 sequence reference getting masked and resulting in an alignment improvement from 11.34% to 4.37% reads with multiple codon alignments.

Masked positions do not contribute to the alignment score and thus possibly lowering it below the minimum threshold; however, we observed no trade-off between optimized reference masking and read mapping percentage (*Figure 3*, panel B). Like *Behrens et al. (2021)*, we observe a striking difference in the mapping of certain tRNA transcripts. For example, transcripts decoding the Ser-UCU codon (AGA anticodon) are lifted out of obscurity (*Figure 3*, panel C). Generally, reference masking appears to increase annotations for around a dozen transcripts but a substantial mapping change only occurs for four codons (*Figure 3—figure Supplement 1*, panel a). The effect of reference masking on the charge measurements was low as expected because this is a relative number (*Figure 3—figure Supplement 1*, panel B).

tRNA modifications are reflected in mismatches, gaps and RT stops Our computational method also supports using misincorporation data for inference of nucleotide modifications which is typically only valid for modifications that disrupt Watson-Crick base pairing such as methylations (*Clark et al., 2016; Behrens et al., 2021*). As such the 5-methoxycarbonylmethyl-2-thiouridine (mcm5s2U) modification should be silent; however, thionucleosides are sensitive to periodate treatment, oxidizing them to sulfonates and making them further sensitive to nucleophilic attack (*Ziff and Fresco, 1968; Rao and Cherayil, 1974*). When periodate oxidation of mcm5s2U is followed by lysine cleavage it would presumably result in a lysine adduct (*Ziff and Fresco, 1968*), thus disrupting Watson-Crick base pairing. We verified this by comparing the misincorporation signature in samples processed with/without periodate oxidation, focusing on the human tRNAs Lys-UUU, Gln-UUG, Glu-UUC and Arg-UCU shown by *Lentini et al. (2018)* to carry be mcm5s2U modification (*Figure 3—figure Supplement 2*). Large changes in the misincorporation signature is observed upon periodate oxidation, but curiously some tRNAs respond with a large decrease in RT readthrough while others see an increase in the mutation and/or gap frequency. Similar observations were recently showed by *Katanski et al. (2022)*.

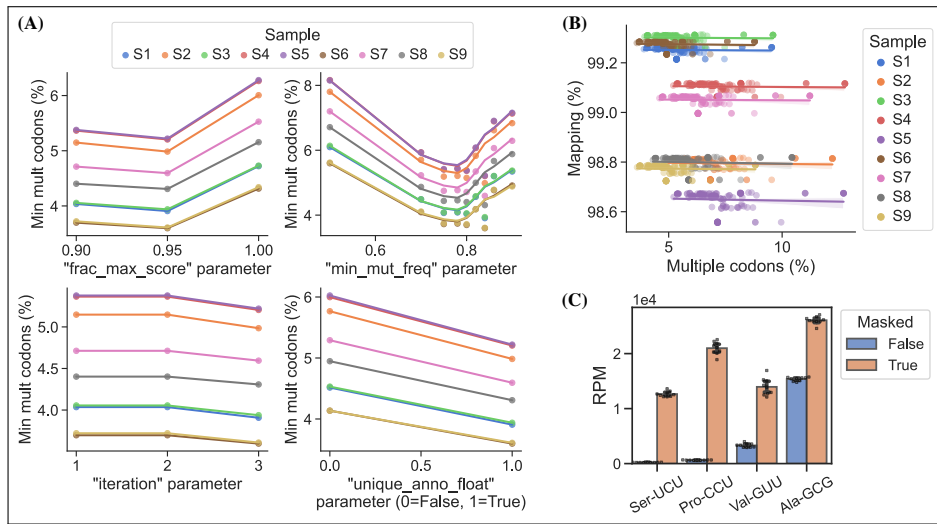


**Figure 3.** Masking of reference tRNA transcript sequences improves alignment performance. **(A)** Grid search optimization of parameters determining the extent of reference masking (see method section for details). Each subplot shows the effect of one tuning parameter when combined with the best combination of the other three. Parameters used for reference masking are chosen to minimize the percentage of reads assigned to tRNAs with multiple codons. **(B)** There is no trade-off between mapping success and multiple codon mapping. **(C)** Reference masking increase RPM values of select codons. RPM levels of the codons shown was found before and after optimized reference masking. Errorbars are bootstrapped 95% confidence interval of the mean over the 9 barcode replicate samples.

**Figure 3—figure supplement 1.** Reference masking effect on RPM and charge levels.

**Figure 3—figure supplement 2.** Anticodon modification mcm5s2U is detected in periodate oxidized samples.

### Barcode replicates show high precision

To assess our measurement precision, we performed our charge tRNA-Seq protocol on the same tRNA sample using all nine barcoded adapters. We used partially deacylated RNA to achieve a representative spread of aminoacetylation levels within a single sample (*Figure 4—figure Supplement 2*, panel A) and then extracted differences compared to the median barcode replicate measurement. When comparing charge measurements binned by barcode, we observed that most were narrowly distributed with the median close to zero indicating little or no barcode bias (*Figure 4*, panel A). Adapter I4Sp is the exception that proves why barcode bias needs to be investigated, because it is consistently overestimating charge levels, with a median overestimate of ~3 percentage points. Overall however, charge measurements show high precision with a standard deviation from the median of just 1.7 percentage points, with similar results at the transcript level (*Figure 4—figure Supplement 1*, panel A).

For RPM values, some barcode replicates were more narrowly distributed than others. However, these differences are small and with a standard deviation from the median of 5.1 percentage we consider the RPM measurements to be precise (*Figure 4*, panel B and *Figure 4—figure Supplement 1*, panel B).

### Charge titration shows high accuracy

Testing the accuracy of charge measurements is a much harder problem. Spiking in a defined ratio of CC and CCA-ending oligo to the ligation reaction is a common approach, but it ignores the possible effect of the Whitfeld reaction. It is also possible to compare to charge measured by Northern blotting, but this presents a different set of issues with probe annealing, band resolution etc. As an alternative, we made a charge titration by mixing different proportions of intact and deacylated RNA allowing us to predict and measure charge levels of over 150 transcripts (*Figure 5*, panel A). The results showed excellent proportionality between predicted and measured charge across the

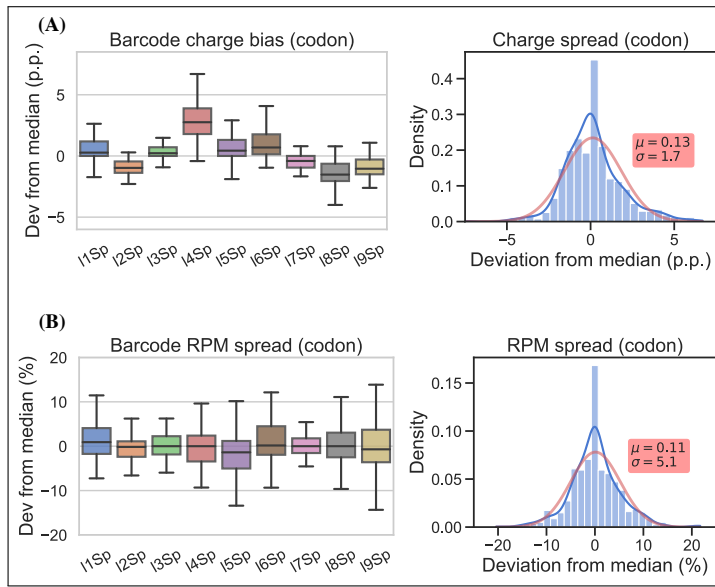


**Figure 4.** Barcode replicates show high precision and no barcode bias. Each of the nine adapters were ligated to the same sample containing a heterogeneous mix of CC and CCA-ending tRNAs. Ligations were then pooled and submitted to the remainder of the charge tRNA-Seq protocol. **(A)** The percentage point deviation from the median charge at the codon level, grouped by barcode identity (left) or shown summarized as a density plot (right). **(B)** The percentage deviation from the median RPM at the codon level, grouped by barcode identity (left) or shown summarized as a density plot (right). Density plots are provided with kernel density estimate (KDE) in blue, normal distribution estimate in red and inserts with mean ( $\mu$ ) and standard deviation ( $\sigma$ ). For plots of transcript level data see *Figure 4—figure Supplement 1*.

**Figure 4—figure supplement 1.** Charge and RPM deviation at the transcript level.

**Figure 4—figure supplement 2.** Best and worst barcode replicates.

full range of values (*Figure 5*, panel B), thus indicating that the charge measurements are highly accurate. This experiment also confirmed our previous observations that barcode bias is limited to the 14Sp adapter which is overestimating charge (*Figure 5*, panel C). Additionally, no bias was found in independently prepared sequencing libraries or any of the different mixing proportions of intact and deacylated RNA (*Figure 5—figure Supplement 2*).

Inspired by *Evans et al. (2017)*, which used radiolabeling techniques to generate a single accurate tRNA charge reference point, we developed a 50% charge control using 3' phosphorylation as protection from periodate oxidation. This control was spiked into samples before the Whitfeld reaction and showed a mean charge of 50.36% and a standard deviation of 1.11 percentage points (*Figure 5—figure Supplement 3*, panel B), thus further validating the measurement accuracy of our method.

**Charge tRNA-Seq enables measurement of aminoacylation half-lives of native tRNAs**  
tRNA aminoacylations are prone to hydrolysis and the effect of pH and temperature on their decay rates has previously been studied (*Hentzen et al., 1972*). Interestingly, *Peacock et al. (2014)* found that the aminoacylation half-life appeared to be determined solely by the identity of the amino acid attachment and not effected significantly by the tRNA sequence or RNA modifications. However, most of the tRNAs used in this study were derived from *in vitro* transcription and only a limited set of RNA modifications were tested; additionally, the study did not cover all 20 native amino acids. Having developed an accurate method for measuring tRNA charge on over a hundred samples in a single sequencing run, we wanted to use this to determine the aminoacylation half-lives of tRNA transcripts with their native RNA modifications.

We used RNA purified from the H1299 cell line, starting at high tRNA charge (*Figure 2*, panel F),

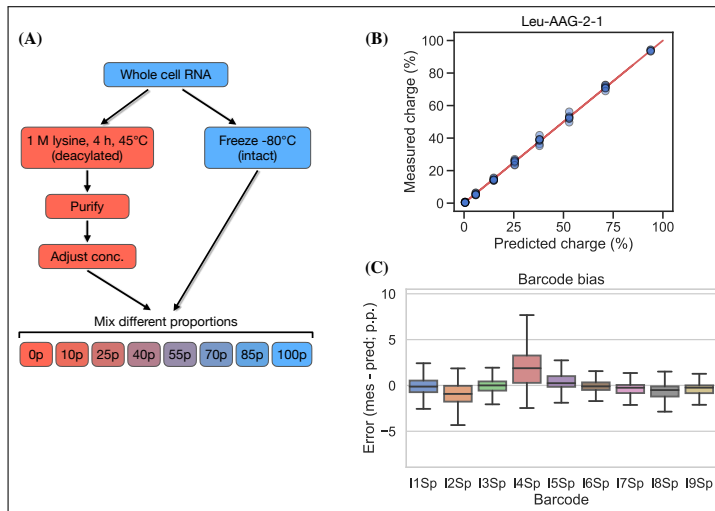


**Figure 5.** Charge titration shows linearity over the full range of charge measurements. **(A)** Schematic illustration of the method to generate samples with predictable charge percentages. **(B)** Titration data for a representative tRNA transcript, Leu-AAG-2-1, with the red line indicating proportionality between predicted and measured charge. For reference, the best and worst fitting tRNA transcripts are shown in *Figure 5—figure Supplement 1*. **(C)** Error binned by adapter barcode. Error is the percentage point difference between the measured vs. predicted charge for all transcripts in the bin.

**Figure 5—figure supplement 1.** Best and worst fitting transcripts for charge titration.

**Figure 5—figure supplement 2.** Error binned by sequencing run and titration sample.

**Figure 5—figure supplement 3.** Spike-in control for 50% charge.

and tracked the aminoacylation decay over time after switching to physiological buffer (pH=7.2) and incubation at 20°C similar to *Peacock et al. (2014)*. After sampling 11 timepoints with 4 replicates, charge measurements for each transcript were fitted to a first-order decay function to estimate the half-life of each transcripts (Supplementary file 4), as exemplified by the representative transcript Arg-TCG-2-1 (*Figure 6*, panel A). When transcripts were grouped by their cognate amino acid, we could confirm that the half-lives are indeed determined mostly by aminoacylation identity and that they span a large 37 fold range (*Figure 6*, panel B). Our half-life estimates are highly correlated with those reported by *Peacock et al. (2014)*, but surprisingly ours appear to be approximately 4 fold higher despite using the same incubation temperature and a similar buffer, with only slightly lower pH (7.2 vs. 7.5; *Figure 6—figure Supplement 1*, panel B).

It seems counterintuitive that the aminoacylation half-life should be completely unaffected by the tRNA sequence; however, as the amino acid is attached to the invariant CCA-end, the nucleotides most proximal to the ester bond are the same for all tRNAs. The most proximal non-invariant nucleotide is the discriminator base. Because we sample all transcripts, we are able to show that the discriminator base is indeed likely to influence the half-life and that a purine base leads to longer half-life than a uracil (*Figure 6*, panel C).

## Discussion

Accurate quantification is a prerequisite for making reliable observations standing the test of time and replication. We have shown a robust method for measuring tRNA charge and done extensive work to validate it in the relevant context of human tRNA. Furthermore, we have quantified the measurement precision of charge and relative expression. Accuracy was only quantified for charge measurement whereas this is more challenging for expression levels (*Fuchs et al., 2015*). One step towards accurate expression level measurements is efficient adapter ligation, such as the splint assisted ligation method used herein; however, future versions of tRNA-Seq should provide better validation and controls for relative expression measurements.

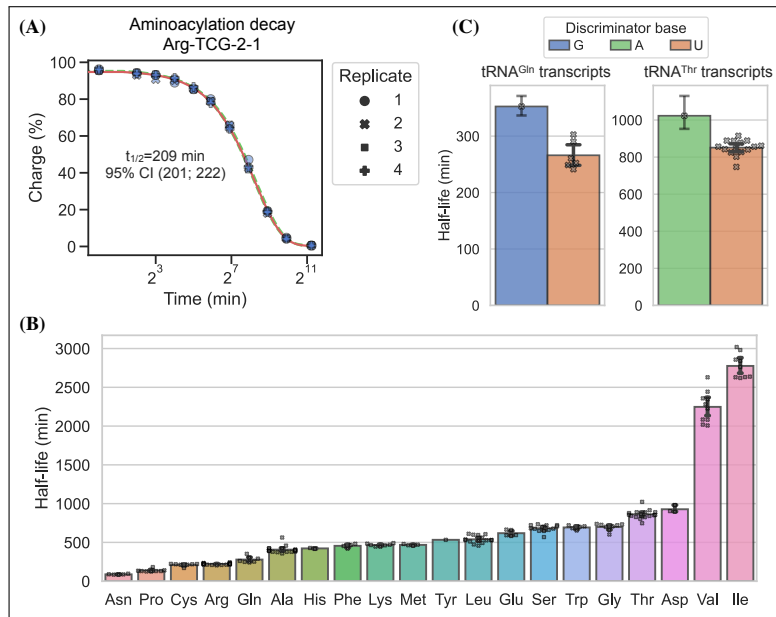


**Figure 6.** Measuring aminoacylation half-life using charge tRNA-Seq. **(A)** Aminoacylation decay for a representative tRNA transcript Arg-TCG-2-1 over the 11 timepoints sampled. For reference, the best and worst fitting tRNA transcripts are shown in *Figure 6—figure Supplement 2*. The fitted first-order decay to estimate the aminoacylation half-life is shown as a red line. Similar dashed lines are plotted in green for the 95% confidence interval (these are hard to see). **(B)** Aminoacylation half-life estimates grouped by amino acid. Each marker represents one transcript, errorbars are bootstrapped 95% confidence intervals of the mean. **(C)** Distribution of aminoacylation half-life estimates for tRNA<sup>Gln</sup> and tRNA<sup>Thr</sup> transcripts grouped by discriminator base identity. Errorbars are bootstrapped 95% confidence intervals. For the single transcripts with G or A discriminator base the bootstrap is performed on measurement replicates while for the U discriminator base it is performed on the transcripts observations.

**Figure 6—figure supplement 1.** RNA integrity and comparison to previous half-life values.

**Figure 6—figure supplement 2.** Best and worst transcript half-life estimates.

288 In our version of the Whitfeld reaction we use lysine to induce base cleavage at low pH. We  
 289 later found that ornithine is an even better inducer of cleavage (*Uziel, 1975*) and thus, the pH of the  
 290 cleavage reaction could be lowered even further and possibly combined with Cu<sup>+2</sup> as a deacylation  
 291 catalyst (*Kroll, 1952; Schofield and Zamecnik, 1968*) to shorten incubation times.

292 In our experience, as well as others (*Shigematsu et al., 2017*), splint assisted ligation is highly  
 293 efficient whereas blunt-end ligation is not. In contrast, *Behrens et al. (2021)* achieved high efficiency  
 294 blunt-end ligation, allowing inclusion of non-mature tRNAs without the normal CCA-end. The  
 295 tRNA<sup>His</sup> is also not suitable for splint assisted ligation due to the additional G added to the 5' end  
 296 (*Heinemann et al., 2012*) and thus shielding the discriminator base from base pairing with the splint.  
 297 Despite this, reads mapping to tRNA<sup>His</sup> are surprisingly abundant and both CC and CCA-ending.  
 298 In future versions of this method, we see the possibility of combining our optimizations with the  
 299 on-bead sample processing developed by *Watkins et al. (2022)* to eliminate gel purification steps  
 300 and achieve faster and cleaner processing.

301 We solve the tRNA alignment problem by non-heuristic alignment which is guaranteed to return  
 302 the best alignment. This is computationally demanding but nevertheless quite possible on the  
 303 small number of tRNA transcript references. A more challenging problem is the application of  
 304 reference masking to improve the annotation accuracy. We used unique codon annotation as the  
 305 objective in our optimization of reference masking, but this is a surrogate as the ground truth cannot  
 306 be determined. Further improvements could be achieved by simulation of tRNA reads including  
 307 realistic RT misincorporations, indels and fall off and optimizing alignment to this simulated ground  
 308 truth. Additionally, annotation performance could be increased further using tools, such as a

309 as hidden Markov models (HMMs), to model complex phenomena such as interaction between  
310 modifications (*Wang et al., 2021; Hernandez-Alias et al., 2022*).

311 In summary, we report a robust charge tRNA-Seq method that has been thoroughly tested and  
312 validated as precise and accurate for charge measurements.

## 313 Methods and Materials

### 314 Cell culture and RNA extraction

315 The human cell line H1299 was acquired from ATCC and tested to be free from mycoplasma  
316 (Mycoprobe, R&D Systems). Cells were maintained in Dulbecco's Modified Eagle's Medium (DMEM)  
317 supplemented with 3.7 g/L sodium bicarbonate, 10% fetal bovine serum (FBS) and 1% penicillin-  
318 streptomycin solution. Cells were incubated in a humidified incubator at 37°C with 5% CO<sub>2</sub>.

319 For RNA extraction, cells were seeded onto a 15 cm dish and grown in DMEM until confluence.  
320 The cells were then removed from the incubator, placed on a slope on ice and media was quickly  
321 and thoroughly aspirated before adding 3 mL Trizol to cover all the cells. From this point onward,  
322 everything was kept ice cold to prevent hydrolysis of the aminoacylation. After a 2 mins incubation,  
323 the cell material was scraped down the slope mixing it with the Trizol, then 2x1.5 mL was transferred  
324 to 2 mL Eppendorf tubes and 0.3 mL chloroform was added. The tubes were vortexed 2 min and  
325 then centrifuged (17,000g, 5 mins). From each tube, 0.75 mL of the upper layer was transferred to  
326 a tube with 0.8 mL isopropanol (IPA), then mixed and incubated 60 mins at -20°C. Tubes were then  
327 centrifuged (17,000g, 15 mins) and RNA pellets were washed twice with 1 mL 80% IPA containing 100  
328 mM sodium acetate (pH=4.5). These washing steps are critical because Trizol contains glycerol which  
329 will react with and inhibit the subsequent periodate oxidation step. A last wash was performed  
330 using 1 mL 100% IPA and after removing the supernatant the RNA pellets were air-dried at room  
331 temperature, then stored dry at -80°C.

### 332 Charge tRNA-Seq using blunt-end ligation

333 For charge tRNA-Seq using blunt-end ligation shown in *Figure 2—figure Supplement 2* the protocol  
334 described by *Behrens et al. (2021)* was followed with the exception of using different adapter  
335 sequences, a UMI containing RT oligo (Supplementary file 1), more rounds of amplification and  
336 gel based size selection for the final sequence library and using paired-end sequencing. Briefly,  
337 whole cell RNA was extracted, reconstituted in 100 mM sodium acetate (pH=4.5) and concentration  
338 adjusted to 1 µg/µL. A 20 µL sample was move to a new tube and submitted to periodate oxidation  
339 and 3' base elimination using sodium borate as described by *Evans et al. (2017)*. After purification  
340 and reconstitution in water, 8 ng of a 50/50 mix of E.coli tRNA-Lys-CCA and E.coli tRNA-Lys-CC oligo  
341 was added as a CCA/CC ratio control. The true ratio of these oligos is hard to control because each  
342 contain a different fraction of truncated oligos that will not contribute to the number of mapped  
343 reads; however, the sequenced CCA/CC ratio is an important measure of the sample to sample  
344 variance. Then the RNA was 3' dephosphorylated using T4 PNK and after another round of RNA  
345 purification the tRNA fraction was isolated on a 10% Urea-TBE gel using SYBRGold staining and  
346 a blue light transilluminator for visualization. After gel elution and reconstitution in water, 100  
347 ng tRNA was transferred to a PCR tube and ligated to 20 pmol pre-adenylated adapter (I1, I2, I3  
348 or I4) in 25% PEG-8000, 1xT4 RNA ligase buffer using 1 µL T4 RNA ligase 2 (truncated KQ) and 1  
349 µL Superaseln. Prior to ligation adapters were adenylated using the NEB 5' DNA Adenylation Kit  
350 following the manufacturers instruction. After purification, adapter adenylation was verified using  
351 differential gel migration. Ligation reactions were incubated 6 h at 25°C, pooled by adapter barcode  
352 and purified, followed by isolation of the ligation product from unligated tRNA using a 10% Urea-TBE  
353 gel.

354 After gel elution and reconstitution in water, the RT-PCR reaction was performed as described  
355 by *Behrens et al. (2021)* using a similar RT oligo but with an extra 9 random nucleotides at the  
356 5'-end to act as a unique molecular identifier (UMI). After the RT-PCR incubation, the remainder of

357 the sample processing follows the charge tRNA-Seq sample processing described below, including  
358 cDNA circularization, Illumina P7/P5 sequence attachment and sequencing.

### 359 Charge tRNA-Seq method optimization

360 Optimization of the oxidation, cleavage and dephosphorylation, collectively called the Whitfeld  
361 reaction *Whitfeld and Markham (1953)*, was done using oligos E.coli tRNA-Lys-UUU-CCA and E.coli  
362 tRNA-Lys-UUU-CC (Supplementary file 1; anticodon omitted from name below). Both oligos were gel  
363 purified on a 10% Urea-TBE gel to resolve full length from truncated oligos. First, the time required  
364 for oxidation was tested, following the same quenching and borax buffered high pH induced  
365 cleavage used by *Evans et al. (2017)*. For this, samples of 35 ng E.coli tRNA-Lys-CCA were prepared  
366 in 10  $\mu$ L 100 mM sodium acetate (pH=4.5) and used as substrate for the Whitfeld reaction conversion  
367 to E.coli tRNA-Lys-CC. Reaction progress was monitored on a 10% Urea-TBE gel by resolving the one  
368 nucleotide difference using the substrate, the product and a 50/50 mix as markers. Also using this  
369 approach, we tested using lysine induced cleavage (*Khym and Cohn, 1961*) by swapping the sodium  
370 borate used for cleavage with 1 M lysine (pH=8). The cleavage step also includes deacylation and  
371 to verify the completeness of this, four samples of 10  $\mu$ g whole cell RNA were prepared in 10  $\mu$ L  
372 100 mM sodium acetate (pH=4.5) and incubated with 50  $\mu$ L 1 M lysine (pH=8) at 45°C for 5, 30, 90  
373 and 270 min. Then, 1 mL ice cold 80% isopropanol containing 100 mM sodium acetate (pH=4.5)  
374 was added, RNA was precipitated, washed twice, dried and reconstituted in 10  $\mu$ L 100 mM sodium  
375 acetate (pH=4.5). These deacylated samples were then submitted to the charge tRNA-Seq sample  
376 processing described below, except using lysine at pH=9.5 and 90 min incubation at 45°C to ensure  
377 complete deacylation. Following this, incubation time in lysine (pH=8) was chosen to be 4 h. To  
378 compare the RNA integrity after cleavage with lysine vs. borax, samples of 10  $\mu$ g whole cell RNA  
379 were prepared in 10  $\mu$ L 100 mM sodium acetate (pH=4.5) and added 50  $\mu$ L of either 1 M lysine  
380 (pH=8) or 100 mM sodium borate (pH=9.5). Tubes were incubated 45°C and samples taken at time  
381 0, 1.5, 4 and 8 h. RNA integrity was determined using TapeStation (high sensitivity RNA) and 10%  
382 Urea-TBE gel . Upon combining the steps of the Whitfeld reaction to a one-pot reaction a color  
383 change was observed after addition of lysine. To test the effect of the periodate quencher, 25  $\mu$ L of  
384 freshly prepared 200 mM NaIO4 in 100 mM sodium acetate (pH=4.5) was quenched by 25  $\mu$ L of  
385 either water (control), glycerol (*Alefelder et al., 1998*), glucose (*Evans et al., 2017*), ribose (*Watkins  
386 et al., 2022*) or uridine at concentrations indicated for 10 min at room temperature. Then 50  $\mu$ L 1 M  
387 lysine at either pH 8 or 9.5 was added and reactions incubated at 45°C for 1 h before moving to  
388 room temperature for visual inspection (*Figure 2—figure Supplement 1*, panel C).

389 For ligation optimization human tRNA was isolated from H1299 cells. First, whole cell RNA was  
390 isolated as described above, reconstituted in water and deacylation at 45°C in 1 M lysine (pH=8) for  
391 4 h. Then RNA was purified using the Monarch RNA Cleanup Kit (50  $\mu$ g) and run on a 10% Urea-TBE  
392 gel to resolve the tRNA from mRNA and rRNA. tRNA was defined as the range between 70 and 85  
393 nt. as approximated by the low range ssRNA ladder. For blunt-end ligations in *Figure 2—figure  
394 Supplement 3*, 40 ng tRNA, either isolated from H1299 cells or as E.coli tRNA-Lys-CC oligo, was  
395 ligated to 20 pmol pre-adenylated adapter in a 20  $\mu$ L reaction containing 25% PEG-8000, 200 U T4  
396 RNA ligase 2 (truncated KQ; Rnl2tr KQ), 10 U SUPERaseln and the vendor provided buffer. For splint  
397 assisted ligation in *Figure 2—figure Supplement 4*, 35 ng tRNA, either isolated from H1299 cells or as  
398 E.coli tRNA-Lys-CC oligo, was ligated to 20 pmol annealed adapter:split partial duplex as described  
399 for charge tRNA-Seq sample processing below. For the non-complementary splint test, two splint  
400 oligos were made with CAAC and AAC overhangs (Supplementary file 1) and annealed to adapter  
401 I1Sp. For the ligation test in *Figure 2*, panel E and *Figure 2—figure Supplement 5*, panel A, 500 ng  
402 tRNA isolated from H1299 cells was subjected to the one-pot Whitfeld reaction described for charge  
403 tRNA-Seq sample processing below but with a single step remove. For the no oxidation sample  
404 NaIO4 was replaces with NaCl, for the no dephosphorylation sample shrimp alkaline phosphatase  
405 (rSAP) was replaces with water and for the no cleavage sample RNA was purified after periodate  
406 quenching. These were compared to a sample processed as described in *Evans et al. (2017)*. All

407 samples were purified using the Monarch RNA Cleanup Kit and 35 ng was used per ligation test  
408 with adapters I1Sp, I2Sp and I3Sp using the ligation protocol described for charge tRNA-Seq sample  
409 processing below.

410 **Charge tRNA-Seq sample processing**

411 Stepwise description with details in Supplementary file 2. Whole cell RNA was reconstituted in  
412 100 mM sodium acetate (pH=4.5) and keep on ice until the end of the periodate oxidation step.  
413 For deacylated control samples, RNA was prepared by first performing a deacylation step on the  
414 input RNA by incubation in 1 M lysine (pH=8) at 45°C for 4 h, followed by purification using the  
415 Monarch RNA Cleanup Kit (50 µg). The RNA concentration was adjusted to 1 µg/µL, 10 µL was  
416 transferred to a fresh tube and 1 µL E.coli tRNA spike-in control was added. Initially, the spike-in  
417 control contained 5 ng/µL E.coli tRNA-Lys-CCA, later 5 ng/µL of each E.coli tRNA-Thr-CGT CCA-Phos  
418 and E.coli tRNA-Thr-CGT CCA was also included. To this 5 µL freshly prepared 200 mM NaIO4 was  
419 added following 10 min incubation on ice, in the dark. For non-oxidized control samples, NaCl  
420 was used instead of NaIO4. The oxidation was quenched by adding 5 µL 50% (v/v) ethylene glycol  
421 (~9 M) and incubating for 5 min on ice and 5 min at room temperate, in the dark. Then 50 µL  
422 1 M lysine (pH=8) with 1 µL Superaseln was added and tubes were incubate for 4 h at 45°C. To  
423 dephosphorylate RNA 8 µL 10X rCutSmart Buffer and 1 µL rSAP was added followed by 30 min  
424 incubation at 37°C. RNA was then purified using the Monarch RNA Cleanup Kit (50 µg), eluting with  
425 30 µL water. A 6 µL sample was then denatured by mixing with 2x urea loading buffer (8 M urea, 30  
426 mM sodium acetate, 2 mM EDTA, 0.02 % (w/v) bromophenol blue and xylene cyanol, pH adjusted to  
427 4.7-5) and incubating 2 min at 90°C. The tRNA fraction was then isolated on a 10% Urea-TBE gel  
428 using SYBRGold staining and a blue light transilluminator for visualization. Gel elution was done by  
429 crushing the gel with a disposable pestle, adding 200 µL gel elution buffer and 1 µL Superaseln,  
430 then snap freezing in liquid nitrogen and incubating at 65°C for 5 mins with shaking. The gel slurry  
431 was filtered through a Spin-X filter following tRNA purification using the Oligo Clean & Concentrator  
432 kit. The concentration of purified tRNA as measured, then it was annealed in NEBuffer 2 by heating  
433 to 94°C for 2 min followed by cooling 1°C/s to 4°C. 35 ng of the annealed tRNA was transferred to a  
434 PCR tube and to this was added 20 pmol annealed adapter:splint partial duplex, 1 µL 10x NEBuffer  
435 2, 2 µL 10x T4 RNA ligase buffer, 4 µL 50% PEG-8000, 1 µL Superaseln and 1 µL T4 RNA ligase 2. The  
436 annealed adapter:splint partial duplex was made by making an equimolar mix of the CCA and CC  
437 splint oligos, then using this to make an equimolar mix with the adapter oligo and annealing this in  
438 NEBuffer 2 by heating to 94°C for 2 min followed by cooling 0.3°C/s to 4°C. Each ligation reaction  
439 was adjusted to 20 µL with water, mixed and incubated 1 h at 37°C followed by 24 h at 4°C and heat  
440 inactivation at 80°C for 5 min. Samples were pooled by adapter barcode, purified using the Oligo  
441 Clean & Concentrator kit and then ligated tRNA was isolated on a gel and purified similarly to the  
442 initial tRNA isolation.

443 Reverse transcription was setup with 60 ng of the purified adapter ligated tRNA as template  
444 using the buffer composition, incubation temperature and time suggested by *Behrens et al. (2021)*.  
445 To 10 µL template in a PCR tube, 2 µL 1.25 µM RT oligo and 4 µL RT buffer was added following  
446 denaturation and annealing by incubation at 90°C for 2 min, 70°C for 30 s and cooling 0.2°C/s to  
447 4°C. Then, to each tube 1 µL 100 mM DTT, 1 µL Superaseln and 1 µL TGIRT-III RT polymerase (or  
448 Maxima H Minus for *Figure 2—figure Supplement 7*) was added following 10 min incubation at  
449 42°C. Then 1 µL 25 mM dNTPs was added and the incubation was resumed at 42°C for 16 h on a  
450 thermocycler with the heated lid set to 50°C. The RNA template was hydrolyzed by adding 1 µL 5 M  
451 NaOH followed by incubation at 95°C for 3 min. The samples were then purified using the Oligo  
452 Clean & Concentrator kit and the cDNA was isolated on a gel and purified similarly to the initial  
453 tRNA isolation, eluting with 7 µL water. cDNA was circularized by transferring 5.5 µL cDNA to a PCR  
454 tube and adding 2 µL 5 M betaine, 1 µL 10x CircLigase buffer, 0.5 µL 1 mM ATP, 0.5 µL 50 mM MnCl2  
455 and 0.5 µL CircLigase. The reaction was incubated at 60°C for 3 h on a thermocycler with a 70°C  
456 heated lid, then the enzyme was deactivated by denaturing at 80°C for 10 min.

457 PCR was used to attach Illumina P7/P5 sequences to flank the tRNA insert. Each PCR reaction  
458 was setup to contain 0.6  $\mu$ L circularized cDNA, 1.5  $\mu$ L 10 mM dNTPs, 5  $\mu$ L 10  $\mu$ M P7 oligo, 5  $\mu$ L 10  
459  $\mu$ M P5 oligo, 10  $\mu$ L 5x KAPA HiFi buffer, 1  $\mu$ L KAPA HiFi polymerase and 26.9  $\mu$ L water. The PCR  
460 reactions were incubated at 95°C for 3 min followed by 3 cycles of 98°C for 20 s, 68°C for 10 s  
461 and 72°C for 15 s, and then followed by X cycles of 98°C for 20 s and 72°C for 15 s, with X being  
462 empirically determined (*Figure 2—figure Supplement 8*, panel A). The optimal number of PCR cycles  
463 were determined by preparing three PCR reactions, incubating them with X=10, 12 and 14 and  
464 running 4  $\mu$ L of each reaction on a 4-12% TBE gel. The PCR reactions with optimal X, resulting  
465 in abundant amplification product with little PCR crossover, were purified using the DNA Clean  
466 & Concentrator-5 kit and resolved on a 4-12% TBE gel. The gel was stained using SYBRGold and  
467 visualized using a blue light transilluminator to isolated the library DNA by cutting out the size range  
468 covering all possible insert lengths (170-290 bp). Gel elution was done by crushing the gel with  
469 a disposable pestle, adding 300  $\mu$ L TBE, snap freezing in liquid nitrogen and incubating at room  
470 temperature overnight with mixing. If necessary, elution time could be decreased by incubation  
471 at higher temperature; although, this required adding higher salt concentrations to prevent DNA  
472 reannealing (*Figure 2—figure Supplement 8*, panel B). The gel slurry was filtered through a Spin-X  
473 filter following DNA purification using the DNA Clean & Concentrator-5 kit and eluting with 20  $\mu$ L  
474 10 mM Tris (pH=8). DNA with different Illumina P7/P5 barcodes were pooled for multiplexing and  
475 sequenced using Illumina paired end sequencing using 2x100 bp reads.

#### 476 E.coli tRNA spike-in control

477 An E.coli tRNA spike-in control was generated from oligos E.coli tRNA-Lys-UUU-CCA and E.coli  
478 tRNA-Thr-CGT-CCAA (anticodon sometimes omitted from name). First, 2  $\mu$ g per well of the E.coli  
479 tRNA-Lys-CCA oligo was loaded on a 10% Urea-TBE gel to resolve full length from truncated oligos.  
480 After gel elution and purification using the Oligo Clean & Concentrator kit the RNA concentration  
481 was measured and adjusted such that 5 ng was spiked into each sample of 10  $\mu$ g whole cell RNA  
482 before periodate oxidation. Adding the control before periodate oxidation afforded an internal  
483 control of the completeness of the oxidation reaction.

484 Second, 30  $\mu$ L of 100  $\mu$ M E.coli tRNA-Thr-CCAA oligo was submitted to a partial Whitfeld reaction,  
485 stopping before the dephosphorylation step. The oxidation reaction was performed by adding 10  
486  $\mu$ L 100 mM sodium acetate (pH=4.5) and 20  $\mu$ L 200 mM NaIO4 followed by incubation for 30 min  
487 at room temperature in the dark. Oxidation was quenched using 20  $\mu$ L 50% ethylene glycol and  
488 incubated 30 min at room temperature in the dark. Then buffer exchange was performed using a P-6  
489 gel column pre-equilibrated with 100 mM lysine (pH=8). To the eluate 400  $\mu$ L 1 M lysine (pH=8) and  
490 1  $\mu$ L Superaseln was added followed by 5 h incubation at 45°C and purification using the Monarch  
491 RNA Cleanup Kit (using two 50  $\mu$ g columns). The product, a 1 nt. truncated and 3' phosphorylated  
492 oligo named E.coli tRNA-Thr-CCA-Phos, was resolved on a gel to isolate the full length oligo, as  
493 described for the other control. Half of this product was submitted to dephosphorylation using  
494 rSAP and purified using the Oligo Clean & Concentrator kit yielding E.coli tRNA-Thr-CCA. Complete  
495 phosphorylation of E.coli tRNA-Thr-CCA-Phos and complete dephosphorylation of E.coli tRNA-Thr-  
496 CCA was verified using ligation (*Figure 5—figure Supplement 3*, panel A). Then concentrations of  
497 both E.coli tRNA-Thr-CCA-Phos and E.coli tRNA-Thr-CCA was measured to generate an equimolar  
498 mix adjusted such that 10 ng was spiked into each sample of 10  $\mu$ g whole cell RNA before periodate  
499 oxidation. The 3' phosphorylation protects from periodate oxidation and thus adding it before  
500 periodate oxidation afforded an internal control of a 50% charged tRNA, probing the completeness  
501 of the whole Whitfeld reaction and potential adapter ligation bias.

#### 502 Oligo design

503 For adapters used for blunt-end ligation the design was similar to *McGlinchy and Ingolia (2017)* and  
504 *Behrens et al. (2021)*, with a 5' phosphorylation to enable adenylation and a 3' dideoxycytidine to  
505 prevent self-ligation and concatemer formation. For adapters I1, I2, I3 and I4 the barcode sequence

506 was 8 nt. starting at the 5', for adapters I1N, I2N and I3N the barcode sequence was truncated  
507 to 5 nt. to make space for a preceding six random nucleotides to diversify the sequence context  
508 engaged in ligation.

509 The design of adapters used for splint assisted ligation was influenced by *Smith et al. (2015)* and  
510 *Shigematsu et al. (2017)* but with several important differences listed below. First, we do not use  
511 ribonucleotides at any positions in our adapters or splint oligos. This affords us higher quality oligos  
512 due to the higher coupling efficiency of deoxyribose during oligo synthesis as well as robustness  
513 against hydrolysis of DNA compared to RNA. A primary reason to use ribonucleotides in the adapters  
514 and splint oligos is to increase ligation efficiency; however, we achieved ~100% ligation efficiency  
515 on isolated human tRNA using our design without ribonucleotides (*Figure 2—figure Supplement 4*,  
516 panel A). Second, instead of ligating the adapter to the 3' and the splint to the 5' of the tRNA, we only  
517 ligate the adapter and block the splint from ligation with a 3' C3 spacer, as well as dephosphorylating  
518 the 5' of the tRNA. Similar to the blunt-end ligation adapters, a 3' dideoxycytidine is included on  
519 all adapters to block self-ligation and concatemer formation. Third, we use two different lengths  
520 splint oligos with overhang compatible to NCCA and NCC-ending tRNA. Fourth, our adapters vary in  
521 length by the size of their barcodes, from 5 to 8 nt. This is to offset the sequencing reading frame  
522 of read P2 (P7) as it progresses into the 3' end of the tRNA, thus increasing the sequence diversity  
523 and base calling quality.

524 The RT-PCR oligo was designed in a similar way as *McGlincy and Ingolia (2017)* and *Behrens*  
525 *et al. (2021)* with a 5' phosphorylation for subsequent circular ligation of the cDNA and an 18-atom  
526 hexa-ethyleneglycol spacer (iSp18) to terminate the polymerase extension and avoiding rolling-  
527 circle amplification during the PCR to attach Illumina P7/P5 sequences. The RT oligo has a random  
528 purine base on the 5' to increase circular ligation efficiency. We added an additional 9 random  
529 nucleotides following this purine to increase the diversity of the sequence engaged in circular  
530 ligation. These random nucleotides also provide a unique molecular identifier (UMI) with 524288  
531 possible sequences that enable collapsing of reads derived from the same tRNA molecule. The  
532 UMI is also used as a general sample quality control by comparing the number of observed UMI  
533 sequences with the number expected. The expected number unique UMI observations is calculated  
534 as:

$$E[X] = n \left[ 1 - \left( \frac{n-1}{n} \right)^k \right] \quad (1)$$

535 With  $E[X]$  being the expected number of unique UMI observations,  $n$  being the number of reads  
536 for the particular sample and  $k$  being the number of possible UMIs.

537 The final dsDNA library was designed as an Illumina TruSeq dual index library with combined i5  
538 and i7 indices attached by PCR with P7/P5 oligos. These oligos were synthesized with a phosphoroth-  
539 ioate bond between the last two nucleotides to prevent degradation by the KAPA HiFi polymerase.  
540 An overview of the RNA/DNA manipulations including ligation of adapters, RT-PCR, circularization  
541 and library PCR is provided in Supplementary file 3.

## 542 Read processing

543 Reads were first demultiplexed according to their i7/i5 barcodes. Read pairs were then trimmed  
544 and merged using AdapterRemoval:

```
545 AdapterRemoval --preserve5p --collapse --minalignmentlength 10 --adapter1  
546     AGATCGGAAGAGCACACGTCTGAACCTCCAGTCAC<P7_index>ATCTCGTATGCCGTCTCTGCTTG --  
547     adapter2 AGATCGGAAGAGCGTCGTAGGGAAAGAGTGT<P5_index>  
548     GTGTAGATCTCGGTGGTCGCCGTATCATT --minlength <MIN_LEN>
```

549 With <P7\_index> and <P5\_index> defined by the i7/i5 index sequences for the given sample  
550 and <MIN\_LEN> set to 25 for charge tRNA-Seq using blunt-end ligation and 39 for charge tRNA-Seq  
551 using splint assisted ligation. Each file with merged reads were then split based on adapter barcode.  
552 A read was assigned to a particular adapter barcode if its 3' end had a substring within a hamming  
553 distance of one to the barcode sequence, including the region complementary to the splint. The

554 adapter sequence was then trimmed off the 3' end; similarly, the 10 nt. UMI was located, saved  
555 and trimmed off the 5' end, leaving only the tRNA sequence with possible 5' non-template bases  
556 introduced during RT-PCR. Finally, samples with an excess of 2e6 reads were downsampled to 2e6  
557 reads.

558 Trimmed reads were aligned to a masked reference as described below using the Smith-  
559 Waterman algorithm implemented by SWIPE (*Rognes, 2011*):

```
560 swipe --symtype 1 --outfmt 7 --num_alignments 3 --num_descriptions 3 --evalue  
561 0.000000001 --strand 1 -G 6 -E 3 --matrix <SCORE_MATRIX>'
```

562 With an input score matrix (<SCORE\_MATRIX>) defining a match score of 1, a mismatch score of -3  
563 and a score for alignment to a masked reference position (N) of 0.

564 Alignment results were processed to extract three key data: 1) tRNA charge, 2) relative expression  
565 level and 3) mismatches, gaps and RT truncations. First the alignment was parsed to extract  
566 transcript annotation(s), alignment score and other relevant information. A read was assigned  
567 the annotation with the highest alignment score and upon ties up to three annotations were  
568 merged. When reporting data on the transcript level, a unique annotation was required for filtering,  
569 when reporting at the codon level multiple annotations were allowed but a unique anticodon was  
570 required and similarly for data on the amino acid level. Relative expression levels were calculated  
571 as reads per million (RPM) with a count correction such that reads with identical sequence and  
572 UMI were only counted once. Charge was calculated using uncorrected counts as this is a relative  
573 number. Mismatches, gaps and RT truncations were extracted by redoing the Smith-Waterman  
574 alignment between the read and its unmasked transcript annotation using a match score of 1, a  
575 mismatch score of -1, a gap opening score of -2 and a gap extension score of -1. Using this new  
576 alignment, mismatched, gaps and the index at the end of the alignment were extracted. Then  
577 for each transcript the fraction of reads having mismatches and gaps at a given position was  
578 calculated and the percentage drop in coverage at each position, referred to here as RT stops. For  
579 both mutation, gap fractions and RT stops the UMI corrected read count was used. We provide a  
580 boilerplate example of the whole read processing workflow on GitHub: [https://github.com/krdav/tRNA-charge-seq/blob/main/projects/example/process\\_data.ipynb](https://github.com/krdav/tRNA-charge-seq/blob/main/projects/example/process_data.ipynb).

## 582 Reference masking

583 A human tRNA transcript reference for alignment was made by downloading the fasta formatted  
584 hg38 high confidence mature tRNA sequences from GtRNAdb (*Chan and Lowe, 2016*). These  
585 sequences were deduplicated and mitochondrial tRNAs and spike-in control sequences were ap-  
586 pended. Then a BLAST database was generated, as required by SWIPE, using the `makeblastdb`  
587 application. To further improve the alignment specificity, a masked reference was made by convert-  
588 ing positions with high likelihood of mismatch to Ns such that these have no negative contribution on  
589 the alignment score. Position-wise mismatch frequency was found as described above and filtered  
590 using a minimum of 200 transcript observations and 100 observations on each position. These  
591 were then turned into a masked reference using four tuning parameters for picking the positions to  
592 mask. `unique_anno`: Only count reads with a unique transcript annotation. `min_mut_freq`: The  
593 minimum mismatch frequency to trigger masking. `frac_max_score`: The minimum fraction of  
594 the maximum alignment score between two reference sequences to expand the masked positions  
595 in one reference to another, requiring both unmasked positions to have the same nucleotide. The  
596 purpose is for an abundant transcript to donate its masking to a highly similar, but less abundant,  
597 transcript likely having the same RNA modifications. `iteration`: The number of masking iterations  
598 to perform. When changing the reference for alignment by masking the annotations can change,  
599 thus changing the position-wise mismatch frequency and the resulting reference masking. Running  
600 multiple iterations of reference masking stabilizes the change.

601 To find the optimal combination of tuning parameters a grid search was performed, testing  
602 all combinations of parameters shown in *Figure 3*, panel A. The objective for the search is to

603 minimize the percentage of reads assigned to transcripts with multiple anticodons. Alternatively,  
 604 the objective could be to minimize the percentage of reads assigned to multiple transcripts; however,  
 605 this objective can lead the tuning parameters towards masking only a single transcript out of a  
 606 family of highly similar transcripts, resulting in assignment of unique annotations to truncated reads,  
 607 which cannot truly distinguish between transcripts of high similarity. This problem is less concerning  
 608 using minimization of multiple anticodons since most families of highly similar transcripts have  
 609 identical anticodons.

### 610 **Barcode replicate test**

611 For the barcode replicate test shown in *Figure 4*, the RNA used was first incubated 8 h at 20°C in  
 612 intracellular physiological buffer, similar to the 8 h timepoint described in the aminoacylation half-  
 613 life section below. This provided tRNA containing a spectrum of charge levels, spanning from almost  
 614 fully acylated isoleucine tRNAs to almost fully deacylated asparagine tRNA. A single 10 µg sample of  
 615 this RNA was then subjected to the one-pot Whitfeld reaction and subsequent tRNA isolation and  
 616 ligation to each of the nine adapters as described for charge tRNA-Seq sample processing above.

### 617 **Charge titration test**

618 Whole cell RNA was reconstituted with 100 mM sodium acetate (pH=4.5) and adjusted to 1 µg/µL  
 619 while keeping the RNA cold throughout. Half of this was moved to a fresh tube and deacylated  
 620 by adding 5x volumes of 1 M lysine (pH=8), incubating at 45°C for 4 h and purifying using the  
 621 Monarch RNA Cleanup Kit. Meanwhile, the other half was stored at -80°C. The concentration of the  
 622 deacylated RNA was adjusted to 1 µg/µL and mixtures of intact and deacylated RNA was made using  
 623 the following percentages of intact/deacylated RNA: 100/0, 85/15, 70/30, 55/45, 40/60, 25/75, 10/90,  
 624 0/100. Then these mixtures were subjected to the charge tRNA-Seq sample processing protocol  
 625 described above with between 4 to 8 barcode replicates across independently prepared sequencing  
 626 libraries, sequenced on different flow cells.

627 Reads were processed and the aminoacylation charge of each transcript was extracted to relate  
 628 the measured with the predicted charge. However, the actual mixing ratios may deviate from the  
 629 ones noted above due to inaccuracies in measuring the RNA concentration of intact and deacylated  
 630 RNA, and due to depletion of certain tRNA species during the deacylation process, for example tRNAs  
 631 sensitive to hydrolysis or depurination. We address this using a correction factor,  $F_i$ , described  
 632 below. To calculate the predicted charge let  $A$  represent intact RNA,  $B$  represent deacylated RNA  
 633 and the index  $i$  represent the transcript. Now, define the concentration,  $C$ , of a tRNA transcript  $i$  in  
 634 the intact RNA as 1, while letting the concentration of the same tRNA transcript in the deacylated  
 635 RNA be a fraction,  $F_i$ , of the intact RNA:

$$C_i^A = 1 \quad (2)$$

$$F_i = \frac{C_i^B}{C_i^A} \Leftrightarrow C_i^B = F_i$$

636 Then, define  $T_i^A$  as the measured charge of the intact tRNA of a transcript  $i$  averaged over the  
 637 replicates, and similarly  $T_i^B$  for deacylated RNA:

$$T_i^A = \text{Avg charge}(A_i) \quad (3)$$

$$T_i^B = \text{Avg charge}(B_i)$$

638 Now, the predicted charge of a mixture of  $A$  and  $B$  can be defined using  $p$  to describe the percentage  
 639 of  $A$  in the mixture:

$$T_i^{AB}(p) = \frac{pT_i^A + (100 - p)T_i^B F_i}{p + (100 - p)F_i} \quad (4)$$

640 In the above, only  $F_i$  is unknown. The titration was made with 8 different mixing ratios, two of  
 641 which are used to calculating  $T_i^A$  and  $T_i^B$ , thus leaving 6 mixing ratios, each with several barcode

replicates, to fit  $F_i$ . Fitting was performed by minimizing the sum of squared differences between predicted and measured charge using the Broyden–Fletcher–Goldfarb–Shanno (BFGS) algorithm with upper and lower bound constraints of 4 and 0.25. Then using **Equation 4** the differences between predicted and measured charge was found and broken down by adapter barcode to investigate ligation bias.

### 647 **Aminoacetylation half-life**

648 Whole cell RNA was reconstituted with 1 mM sodium acetate (pH=4.5) and adjusted to 1.5 µg/µL  
649 while keeping the RNA cold throughout. A zero timepoint was then taken and 80 µL was transferred  
650 to a PCR tube after which the experiment was started by adding 20 µL room temperature 5x  
651 buffer, quickly mixing and placing the tube on a thermocycler set to 20°C. The buffer used was  
652 an intracellular physiological buffer at 1x containing: 19 mM NaCl, 125 mM KCl, 0.33 mM CaCl<sub>2</sub>,  
653 1.4 mM MgCl<sub>2</sub>, 0.5 mM spermidine, 30 mM HEPES, adjusted to pH=7.2 with KOH. Time from start  
654 of incubation was tracked and samples drawn at the following timepoints: 4 min, 8 min, 16 min,  
655 32 min, 1 h, 2 h, 4 h, 8 h, 16 h and 40 h. For the 40 h timepoint, two samples were drawn: one  
656 standard and one receiving sham (NaCl) oxidation. Sample were taken by removing 8 µL, mixing it  
657 in a prepared tube with 2 µL ice cold 500 mM sodium acetate (pH=4.5) and storing it at -80°C until  
658 all timepoints were collected. This was repeated four times to generate independent replicates.  
659 Then samples were processed similar to the charge tRNA-Seq protocol described above, but with  
660 the three 5 min incubation times during oxidation and quenching increased to 30 min each due to  
661 the lower periodate solubility in the presence of potassium ions.

662 After read processing and alignment, data integrity was verified by checking that the E.coli tRNA  
663 spike-in control and the non-oxidized 40 h samples conformed to expectations. RNA integrity at  
664 the end of the experiment was also verified on a gel (**Figure 6—figure Supplement 1**, panel A). The  
665 aminoacylation charge was then calculated at the codon level and the data fitted to an equation  
666 describing first-order decay:

$$N(t) = N_0 \left( \frac{1}{2} \right)^{\frac{t}{t_{1/2}}} + N_\infty \quad (5)$$

667 Where  $N(t)$  is the charge of a given codon as a function of time,  $N_0$  is the charge at time zero and  
668  $t_{1/2}$  is the decay half-life. We added the  $N_\infty$  parameter to model the lower asymptote of charge to  
669 accommodate the small fraction of tRNAs that still presents with a CCA-end after full deacylation.  
670 The three parameters were fitted to the data by minimizing the sum of squared errors using the  
671 Broyden–Fletcher–Goldfarb–Shanno (BFGS) algorithm with upper and lower bound constraints for  
672  $N_0$  between 100 and 0 percent, for  $t_{1/2}$  between 1e5 and 1 min and for  $N_\infty$  between 3.5 and 0 percent.  
673 A point estimate for the three parameters were found using all timepoints and replicates and a  
674 95% confidence interval was found using bootstrapping (N=1000) by sampling a single time-series  
675 made up of random draws from the replicates (Supplementary file 4).

### 676 **Data availability**

677 Plots with Seaborn. Boxplots are plotting with quartile boxes and whiskers covering the remainder  
678 of datapoints within a maximum of 1.5 times the inter-quartile range.

679 Raw data and code for processing uploaded to: [some data dump link]

680 Python code available on Github: [github.com/krdav/tRNA-charge-seq](https://github.com/krdav/tRNA-charge-seq)

### 681 **Acknowledgments**

682 We would like to acknowledge Arvind Rasi Subramaniam for suggesting we setup charge tRNA-seq,  
683 Alicia Darnell for sharing relevant samples and data and David Sokolov for help with early method  
684 optimization.

685    **Funding**

686    L.B.S. acknowledges support from the National Institute of General Medical Sciences (NIGMS;  
687    R35GM147118).

688    **References**

- 689    Alefelder S, Patel BK, Eckstein F. Incorporation of terminal phosphorothioates into oligonucleotides. Nucleic  
690    Acids Res. 1998 Nov; 26(21):4983–4988.
- 691    Behrens A, Rodschinka G, Nedalkova DD. High-resolution quantitative profiling of tRNA abundance and  
692    modification status in eukaryotes by mim-tRNAseq. Mol Cell. 2021 Feb; .
- 693    Chan PP, Lowe TM. GtRNAdb 2.0: an expanded database of transfer RNA genes identified in complete and  
694    draft genomes. Nucleic Acids Res. 2016 Jan; 44(D1):D184–9.
- 695    Clark WC, Evans ME, Dominissini D, Zheng G, Pan T. tRNA base methylation identification and quantification via  
696    high-throughput sequencing. RNA. 2016 Nov; 22(11):1771–1784.
- 697    Cozen AE, Quartley E, Holmes AD, Hrabeta-Robinson E, Phizicky EM, Lowe TM. ARM-seq: AlkB-facilitated RNA  
698    methylation sequencing reveals a complex landscape of modified tRNA fragments. Nat Methods. 2015 Sep;  
699    12(9):879–884.
- 700    Dittmar KA, Sørensen MA, Elf J, Ehrenberg M, Pan T. Selective charging of tRNA isoacceptors induced by  
701    amino-acid starvation. EMBO Rep. 2005 Feb; 6(2):151–157.
- 702    Dyer JR. Use of periodate oxidations in biochemical analysis. Methods Biochem Anal. 1956; 3:111–152.
- 703    Erber L, Hoffmann A, Fallmann J, Betat H, Stadler PF, Mörl M. LOTTE-seq (Long hairpin oligonucleotide based tRNA  
704    high-throughput sequencing): specific selection of tRNAs with 3'-CCA end for high-throughput sequencing.  
705    RNA Biol. 2020 Jan; 17(1):23–32.
- 706    Erskine JWB, Strouts CRN, Walley G, Lazarus W. A simple volumetric method for the routine determination of  
707    glycerol. Analyst. 1953 Jan; 78(932):630–636.
- 708    Evans ME, Clark WC, Zheng G, Pan T. Determination of tRNA aminoacylation levels by high-throughput sequencing.  
709    Nucleic Acids Res. 2017 Aug; 45(14):e133.
- 710    Fuchs RT, Sun Z, Zhuang F, Robb GB. Bias in ligation-based small RNA sequencing library construction is  
711    determined by adaptor and RNA structure. PLoS One. 2015 May; 10(5):e0126049.
- 712    Heinemann IU, Nakamura A, O'Donoghue P, Eiler D, Söll D. tRNAHis-guanylyltransferase establishes tRNAHis  
713    identity. Nucleic Acids Res. 2012 Jan; 40(1):333–344.
- 714    Hentzen D, Mandel P, Garel JP. Relation between aminoacyl-tRNA stability and the fixed amino acid. Biochim  
715    Biophys Acta. 1972 Oct; 281(2):228–232.
- 716    Hernandez-Alias X, Katanski CD, Zhang W, Assari M, Watkins CP, Schaefer MH, Serrano L, Pan T. Single-read  
717    tRNA-seq analysis reveals coordination of tRNA modification and aminoacylation and fragmentation. Nucleic  
718    Acids Res. 2022 Dec; .
- 719    Ho YS, Kan YW. In vivo aminoacylation of human and Xenopus suppressor tRNAs constructed by site-specific  
720    mutagenesis. Proc Natl Acad Sci U S A. 1987 Apr; 84(8):2185–2188.
- 721    Hoffmann A, Fallmann J, Vilardo E, Mörl M, Stadler PF, Amman F. Accurate mapping of tRNA reads. Bioinformatics.  
722    2018 Apr; 34(7):1116–1124.
- 723    Holcomb CL, Rastrou M, Williams TC, Goodridge D, Lazaro AM, Tilanus M, Erlich HA. Next-generation sequencing  
724    can reveal in vitro-generated PCR crossover products: some artifactual sequences correspond to HLA alleles  
725    in the IMGT/HLA database. Tissue Antigens. 2014 Jan; 83(1):32–40.
- 726    Jayaprakash AD, Jabado O, Brown BD, Sachidanandam R. Identification and remediation of biases in the activity  
727    of RNA ligases in small-RNA deep sequencing. Nucleic Acids Res. 2011 Nov; 39(21):e141.
- 728    Katanski CD, Watkins CP, Zhang W, Reyer M, Miller S, Pan T. Analysis of queuosine and 2-thio tRNA modifications  
729    by high throughput sequencing. Nucleic Acids Res. 2022 Sep; 50(17):e99.

- 730    **Khym JX**, Cohn WE. Amine-induced cleavage of periodate-oxidized nucleotide residues. *J Biol Chem.* 1961 Mar; 236:PC9–10.
- 732    **Khym JX**, Uziel M. The use of the cetyltrimethylammonium cation in terminal sequence analyses of ribonucleic acids. *Biochemistry.* 1968 Jan; 7(1):422–426.
- 734    **Kroll H.** The Participation of Heavy Metal Ions in the Hydrolysis of Amino Acid Esters1. *J Am Chem Soc.* 1952 Apr; 74(8):2036–2039.
- 736    **Langmead B**, Salzberg SL. Fast gapped-read alignment with Bowtie 2. *Nat Methods.* 2012 Mar; 9(4):357–359.
- 737    **Langmead B**, Trapnell C, Pop M, Salzberg SL. Ultrafast and memory-efficient alignment of short DNA sequences to the human genome. *Genome Biol.* 2009 Mar; 10(3):R25.
- 739    **Lentini JM**, Ramos J, Fu D. Monitoring the 5-methoxycarbonylmethyl-2-thiouridine (mcm5s2U) modification in eukaryotic tRNAs via the  $\gamma$ -toxin endonuclease. *RNA.* 2018 May; 24(5):749–758.
- 741    **Lucas MC**, Pryszcz LP, Medina R, Milenkovic I, Camacho N, Marchand V, Motorin Y, Ribas de Pouplana L, Novoa EM. Quantitative analysis of tRNA abundance and modifications by nanopore RNA sequencing. *Nat Biotechnol.* 2023 Apr; p. 1–15.
- 744    **McGlinny NJ**, Ingolia NT. Transcriptome-wide measurement of translation by ribosome profiling. *Methods.* 2017 Aug; 126:112–129.
- 746    **Mohr S**, Ghanem E, Smith W, Sheeter D, Qin Y, King O, Polioudakis D, Iyer VR, Hunicke-Smith S, Swamy S, Kuersten S, Lambowitz AM. Thermostable group II intron reverse transcriptase fusion proteins and their use in cDNA synthesis and next-generation RNA sequencing. *RNA.* 2013 Jul; 19(7):958–970.
- 749    **Motorin Y**, Muller S, Behm-Ansmant I, Brannant C. Identification of Modified Residues in RNAs by Reverse Transcription-Based Methods. In: *Methods in Enzymology*, vol. 425 Academic Press; 2007.p. 21–53.
- 751    **Neu HC**, Heppel LA. NUCLEOTIDE SEQUENCE ANALYSIS OF POLYRIBONUCLEOTIDES BY MEANS OF PERIODATE OXIDATION FOLLOWED BY CLEAVAGE WITH AN AMINE. *J Biol Chem.* 1964 Sep; 239:2927–2934.
- 753    **Pavlova NN**, King B, Josselsohn RH, Violante S, Macera VL, Vardhana SA, Cross JR, Thompson CB. Translation in amino-acid-poor environments is limited by tRNAGln charging. *Elife.* 2020 Dec; 9.
- 755    **Peacock JR**, Walvoord RR, Chang AY, Kozlowski MC, Gamper H, Hou YM. Amino acid-dependent stability of the acyl linkage in aminoacyl-tRNA. *RNA.* 2014 Jun; 20(6):758–764.
- 757    **Pinkard O**, McFarland S, Sweet T, Coller J. Quantitative tRNA-sequencing uncovers metazoan tissue-specific tRNA regulation. *Nat Commun.* 2020 Aug; 11(1):4104.
- 759    **Rammler DH.** Periodate oxidations of enamines. I. Oxidation of adenosine 5'-monophosphate in the presence of methylamine. *Biochemistry.* 1971 Dec; 10(25):4699–4705.
- 761    **Rao YS**, Cherayil JD. Studies on chemical modification of thionucleosides in the transfer ribonucleic acid of *Escherichia coli*. *Biochem J.* 1974 Nov; 143(2):285–294.
- 763    **Rognes T.** Faster Smith-Waterman database searches with inter-sequence SIMD parallelisation. *BMC Bioinformatics.* 2011 Jun; 12:221.
- 765    **Saraiva MA**, Borges CM, Florêncio MH. Reactions of a modified lysine with aldehydic and diketonic dicarbonyl compounds: an electrospray mass spectrometry structure/activity study. *J Mass Spectrom.* 2006 Feb; 41(2):216–228.
- 768    **Sas-Chen A**, Schwartz S. Misincorporation signatures for detecting modifications in mRNA: Not as simple as it sounds. *Methods.* 2019 Mar; 156:53–59.
- 770    **Schofield P**, Zamecnik PC. Cupric ion catalysis in hydrolysis of aminoacyl-tRNA. *Biochim Biophys Acta.* 1968 Feb; 155(2):410–416.
- 772    **Shigematsu M**, Honda S, Loher P, Telonis AG, Rigoutsos I, Kirino Y. YAMAT-seq: an efficient method for high-throughput sequencing of mature transfer RNAs. *Nucleic Acids Res.* 2017 May; 45(9):e70.
- 774    **Smith AM**, Abu-Shumays R, Akeson M, Bernick DL. Capture, Unfolding, and Detection of Individual tRNA Molecules Using a Nanopore Device. *Front Bioeng Biotechnol.* 2015 Jun; 3:91.

- 776 **Stenum TS**, Sørensen MA, Svenningsen SL. Quantification of the Abundance and Charging Levels of Transfer  
777 RNAs in Escherichia coli. *J Vis Exp.* 2017 Aug; 1(126).
- 778 **Thomas NK**, Poodari VC, Jain M, Olsen HE, Akeson M, Abu-Shumays RL. Direct Nanopore Sequencing of Individual  
779 Full Length tRNA Strands. *ACS Nano.* 2021 Oct; 15(10):16642–16653.
- 780 **Tsukamoto Y**, Nakamura Y, Hirata M, Sakate R, Kimura T. i-tRAP (individual tRNA acylation PCR): A convenient  
781 method for selective quantification of tRNA charging. *RNA.* 2022 Oct; 29(1):111–122.
- 782 **Uziel M**. Amine-catalyzed elimination of beta-phosphoric esters from aldehydes derived from ribonucleic acid  
783 and model substrates. *Arch Biochem Biophys.* 1975 Jan; 166(1):201–212.
- 784 **Uziel M**. Periodate oxidation and amine-catalyzed elimination of the terminal nucleoside from adenylate or  
785 ribonucleic acid. Products of overoxidation. *Biochemistry.* 1973; 12(5):938–942.
- 786 **Varshney U**, Lee CP, RajBhandary UL. Direct analysis of aminoacylation levels of tRNAs in vivo. Application to  
787 studying recognition of Escherichia coli initiator tRNA mutants by glutaminyl-tRNA synthetase. *J Biol Chem.*  
788 1991 Dec; 266(36):24712–24718.
- 789 **Wang J**, Toffano-Nioche C, Lorieux F, Gautheret D, Lehmann J. Accurate characterization of Escherichia coli tRNA  
790 modifications with a simple method of deep-sequencing library preparation. *RNA Biol.* 2021 Jan; 18(1):33–46.
- 791 **Warren JM**, Salinas-Giegé T, Hummel G, Coots NL, Svendsen JM, Brown KC, Drouard L, Sloan DB. Combining  
792 tRNA sequencing methods to characterize plant tRNA expression and post-transcriptional modification. *RNA Biol.*  
793 2021 Jan; 18(1):64–78.
- 794 **Watkins CP**, Zhang W, Wylder AC, Katanski CD, Pan T. A multiplex platform for small RNA sequencing elucidates  
795 multifaceted tRNA stress response and translational regulation. *Nat Commun.* 2022 May; 13(1):2491.
- 796 **Whitfeld PR**. A method for the determination of nucleotide sequence in polyribonucleotides. *Biochem J.* 1954  
797 Nov; 58(3):390–396.
- 798 **Whitfeld PR**, Markham R. Natural configuration of the purine nucleotides in ribonucleic acids; chemical  
799 hydrolysis of the dinucleoside phosphates. *Nature.* 1953 Jun; 171(4365):1151–1152.
- 800 **Wolfson AD**, Uhlenbeck OC. Modulation of tRNA<sup>A<sub>1a</sub></sup> identity by inorganic pyrophosphatase. *Proc Natl Acad Sci  
801 U S A.* 2002 Apr; 99(9):5965–5970.
- 802 **Yamagami R**, Hori H. Application of mutational profiling: New functional analyses reveal the tRNA recognition  
803 mechanism of tRNA m1A22 methyltransferase. *J Biol Chem.* 2022 Dec; 299(1):102759.
- 804 **Zheng G**, Qin Y, Clark WC, Dai Q, Yi C, He C, Lambowitz AM, Pan T. Efficient and quantitative high-throughput  
805 tRNA sequencing. *Nat Methods.* 2015 Sep; 12(9):835–837.
- 806 **Zhuang F**, Fuchs RT, Sun Z, Zheng Y, Robb GB. Structural bias in T4 RNA ligase-mediated 3'-adapter ligation.  
807 *Nucleic Acids Res.* 2012 Apr; 40(7):e54.
- 808 **Ziff EB**, Fresco JR. Chemical transformation of 4-thiouracil nucleosides to uracil and cytosine counterparts. *J Am  
809 Chem Soc.* 1968 Dec; 90(26):7338–7342.

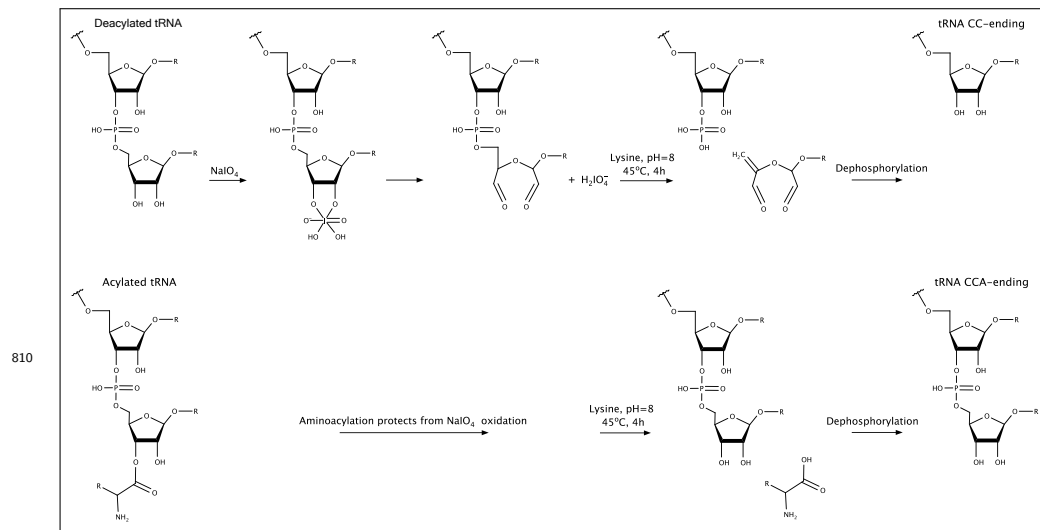


**Figure 1—figure supplement 1.** Schematic of the Whitfeld reaction with acylated and deacylated tRNA leading to generation of CCA and CC-ending tRNAs. For deacylated tRNA, 3' adenosine is oxidized by periodate and then cleaved off by lysine induced  $\beta$ -elimination [references]. Acylated tRNA is protected from periodate oxidation but will be deacylated in the subsequent incubation with lysine.

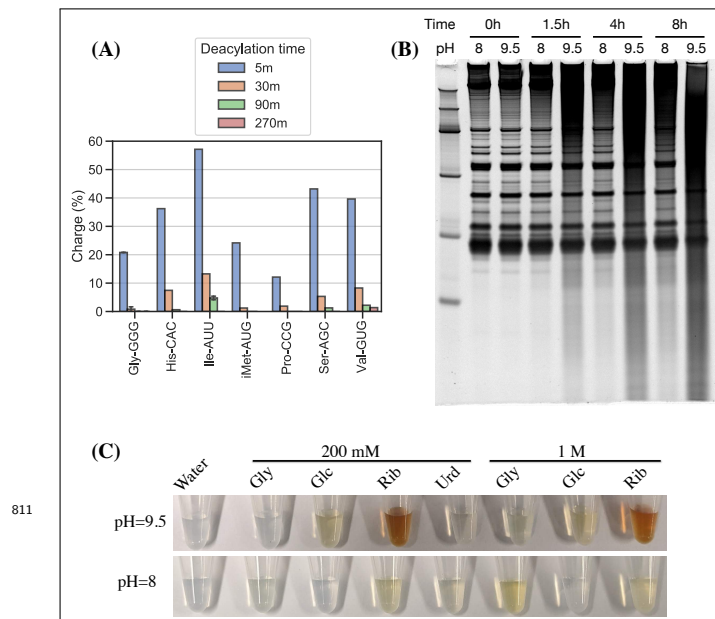


**Figure 2—figure supplement 1.** Optimizing lysine induced cleavage for the charge tRNA-Seq method. **(A)** Measured aminoacylation level after 5, 30, 90 and 270 min of deacylation in 1 M lysine pH=8 at 45°C. After deacylation, RNA was purified and submitted to the Whitfeld reaction using lysine cleavage at pH=9.5 for 90 min at 45°C to ensure complete deacylation. The RNA was then processed using the described charge tRNA-Seq method. **(B)** RNA stability over time for lysine cleavage at pH=8 and borax cleavage at pH=9.5. **(C)** Lysine reacts with dialdehydes forming from quencher oxidation. One-pot Whitfeld reactions were performed at pH=8 and pH=9.5 and quenched with either glycerol (Gly), glucose (Glc), ribose (Rib) or uridine (Urd) at concentrations indicated. Pictures taken after the lysine cleavage step indicate side product formation consistent with lysine reacting with dialdehydes formed during the periodate quenching (*Saraiva et al., 2006*). This side product causes problems in the later purification step.

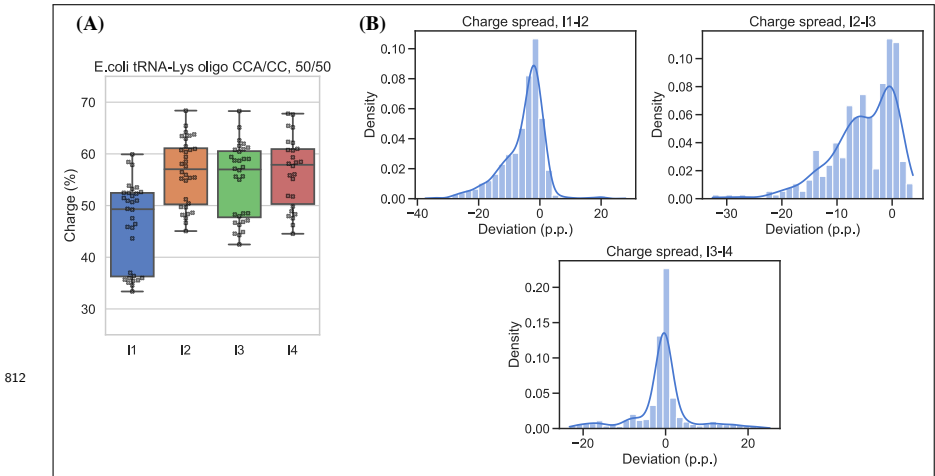


**Figure 2—figure supplement 2.** Measurement bias in charge tRNA-Seq using blunt-end ligation. **(A)** Measured charge of a E.coli tRNA-Lys oligo control spiked into samples processed with four different pre-adenylated adapters using the method described by *Behrens et al. (2021)*. The control was made using a mix of 50% E.coli tRNA-Lys-CCA and 50% E.coli tRNA-Lys-CC and thus its charge does not refer to aminoacylation but the CCA/CC ratio. **(B)** Distribution of charge differences at the transcript level among samples with two barcode replicates, comparing adapters I1 vs. I2, I2 vs. I3 and I3 vs. I4. Deviation is reported as percentage points and the kernel density estimate (KDE) is overlaid.

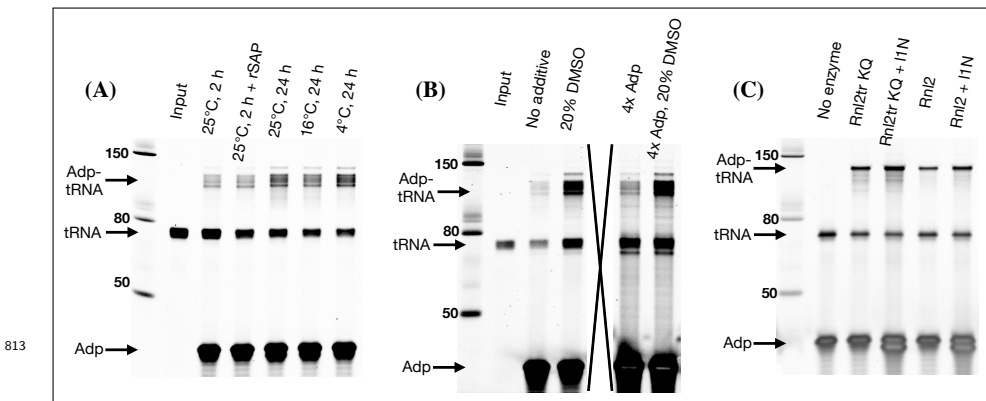


**Figure 2—figure supplement 3.** Despite optimization attempts, high ligation efficiency could not be achieved for blunt-end ligation. **(A)** Effect of incubation temperature, time and addition of a phosphatase (rSAP). Using deacylated and gel purified human tRNA as substrate and pre-adenylated I3N as adapter, otherwise following the method in *Behrens et al. (2021)*. **(B)** Effect of additives and higher adapter concentration. Using deacylated and gel purified human tRNA as substrate, pre-adenylated I2N as adapter and 4°C, 24 h incubation. An irrelevant well has been crossed out to avoid image splicing. **(C)** Effect of ligase type. Using the E.coli tRNA-Lys-CCA oligo as substrate, pre-adenylated I1N as adapter and 4°C, 24 h incubation with 20% DMSO.

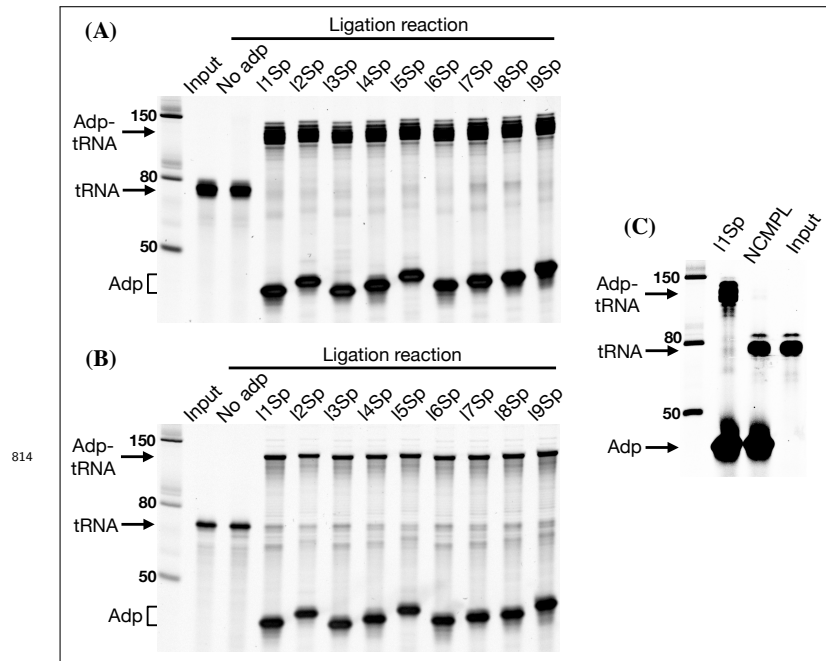


**Figure 2—figure supplement 4.** Ligation efficiency of all the barcoded adapters is high but depends on splint complementarity. **(A)** Ligation reactions using deacylated purified human tRNA as substrate. **(B)** Ligation reactions using E.coli tRNA-Lys-CC oligo as substrate. **(C)** Comparing ligation using a tRNA-end complementary splint (11Sp lane) vs. a non-complementary splint (NCMPL lane). For both ligations the 11Sp adapter was used. For the non-complementary splint ligation the two standard TGGN and GGN overhang generating splints were swapped by two splints generating CAAC and AAC overhangs.

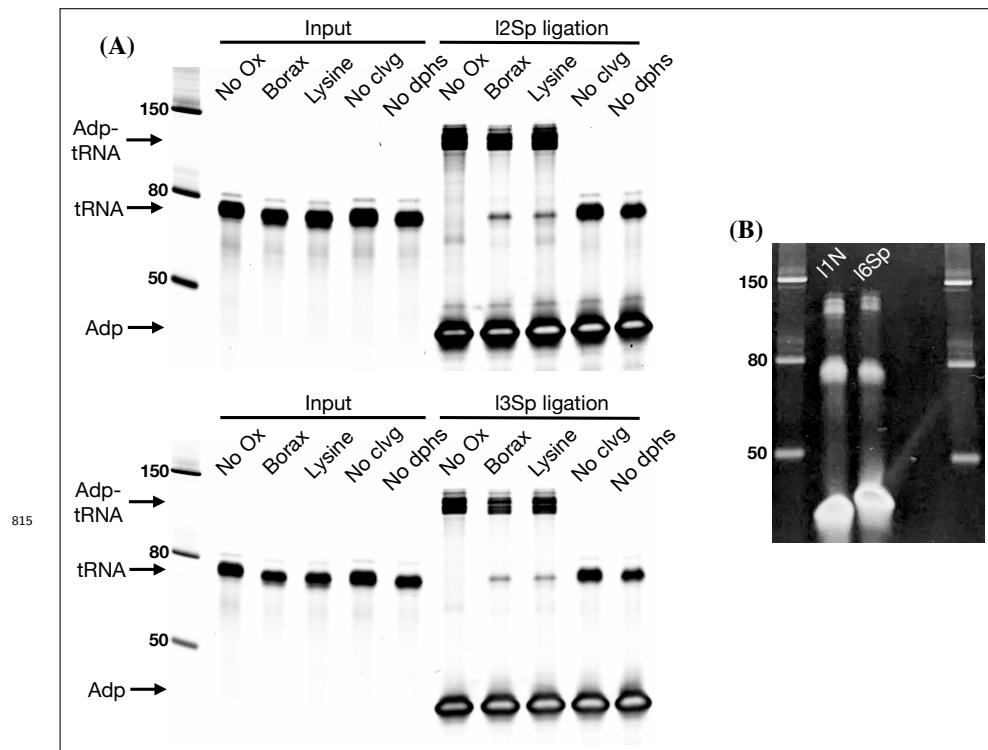


**Figure 2—figure supplement 5.** **(A)** Ligation test comparing the effect of RNA processing. Similar to **Figure 2**, panel E but with two different adapters. **(B)** The unligated tRNA that arises after tRNA is oxidized with periodate in panel A is refractory to further ligation. The unligated tRNA was gel purified from enough ligation reactions as shown in panel A to setup two new ligation reactions using either I1N pre-adenylated adapter for blunt end ligation or I6Sp for splint assisted ligation. For I1N, ligation was setup with 35 ng tRNA, 20 pmol adapter, 17.5% PEG-8000, 20% DMSO, 1xT4 RNA ligase buffer, 1  $\mu$ L T4 RNA ligase 2 (truncated KQ) and 1  $\mu$ L Superaseln. For I6Sp, the ligation was setup as described in the charge tRNA-Seq protocol.

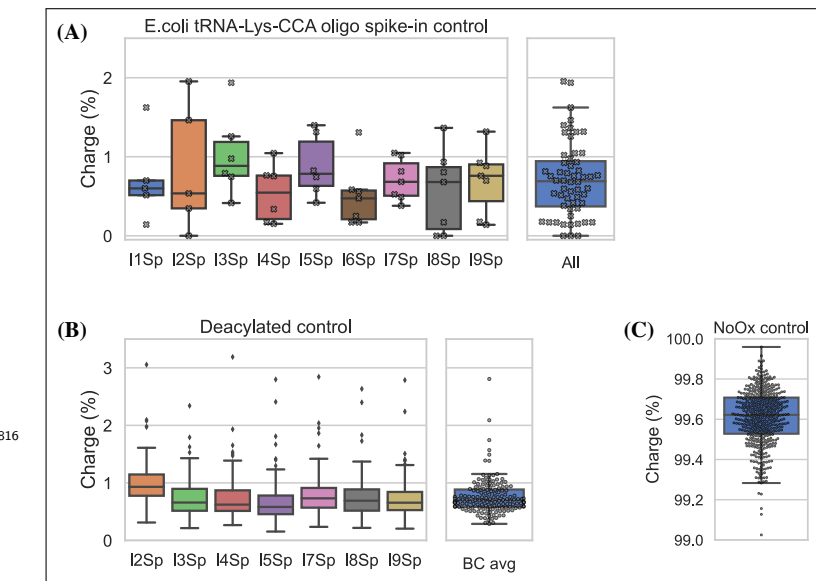


**Figure 2—figure supplement 6.** Charge tRNA-Seq control samples and spike-ins validate method. **(A)** Cleavage of the 3' adenosine on spike-in oligo is near complete. Using the E.coli tRNA-Lys-CCA oligo as a spike-in control to monitor completion of the Whitfeld reaction. If complete, 100% E.coli tRNA-Lys-CC should be produced and thus appearing as 0% charged. **(B)** Aminoacylation level of tRNA transcripts after undergoing deacylation by incubation at 45°C for 4 h in 1 M lysine (pH=8). Mitochondrial tRNA<sup>fMet</sup> was excluded because formylated or acetylated amino acids are known to be highly resistant towards deacylation (*Schofield and Zamecnik, 1968*). **(C)** Aminoacylation level of tRNA transcripts from four samples receiving sham oxidation (NaCl) during the Whitfeld reaction.

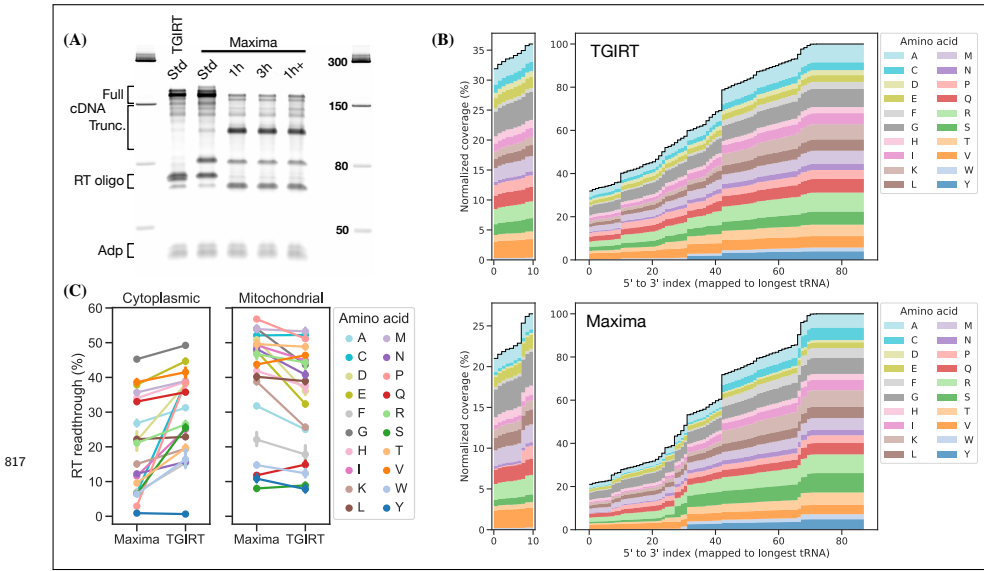


**Figure 2—figure supplement 7. (A)** The Maxima RT polymerase produces similar levels of full size cDNA as TGIRT-III under the standard (Std) tRNA-Seq RT-PCR conditions ( $42^{\circ}\text{C}$ , 16 h, suggested by *Behrens et al. (2021)*). For Maxima, other incubation conditions tested are: 1 h at  $60^{\circ}\text{C}$  (similar to *Lucas et al. (2023)*), 3 h at  $60^{\circ}\text{C}$  and 1 h at  $60^{\circ}\text{C}$  followed by 15 h at  $42^{\circ}\text{C}$  (1h+). After RT-PCR, the RNA template was remove by NaOH hydrolysis, liberating the DNA adapter annotated on the gel. **(B)** Coverage plots for cytoplasmic tRNA transcripts grouped by cognate amino acid, comparing samples prepared with TGIRT-III or Maxima using standard incubation ( $42^{\circ}\text{C}$ , 16 h). **(C)** Percentage of full length transcripts grouped by cognate amino acid (i.e. left side of plots in panel B). Errorbars are bootstrapped 95% confidence interval of the mean over the 7 individual samples barcoded, pooled and used for RT-PCR template with both TGIRT-III and Maxima.

817

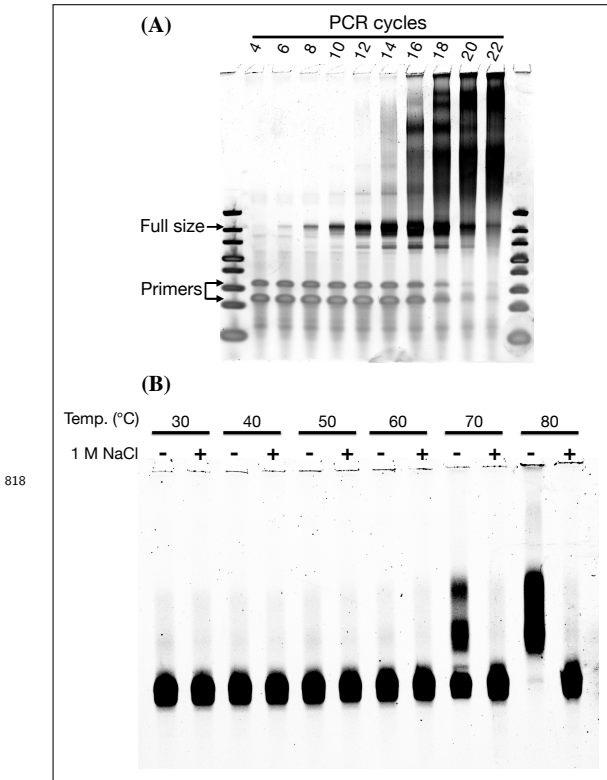


**Figure 2—figure supplement 8.** (A) The specificity of the final library PCR step (attaching Illumina P7 and P5 sequences) deteriorates with increasing product-to-primer ratios, probably due to high tRNA homology and PCR crossover (*Holcomb et al., 2014*). (B) tRNA-Seq DNA library reannealing is inhibited by high salt concentrations. A gel purified charge tRNA-Seq DNA library was resuspended in TBE buffer and incubated 30 min at different temperatures with or without 1 M NaCl.

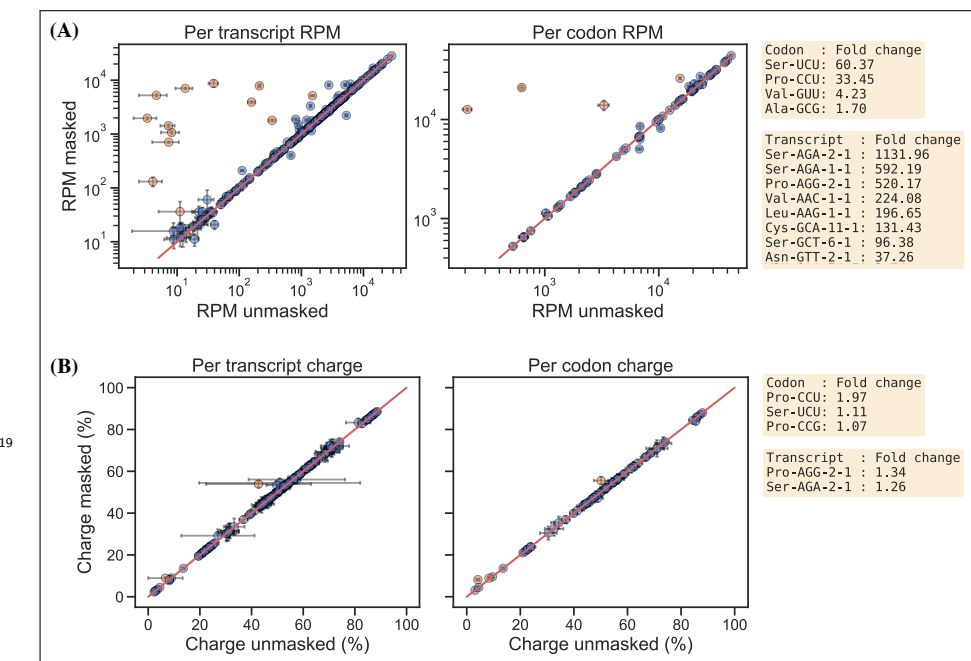


**Figure 3—figure supplement 1.** **(A)** Reference masking effect on RPM levels per transcripts (left) and per codon (right). Transcript points showing > 3, and codon points showing > 1.5, fold increase or decrease upon reference masking are colored orange. The highest fold change transcripts and codons are annotated on the right side of the plot. **(B)** Reference masking effect on charge levels per transcripts (left) and per codon (right). Points showing > 1.05 fold increase or decrease upon reference masking are colored orange and annotated on the right side of the plot.

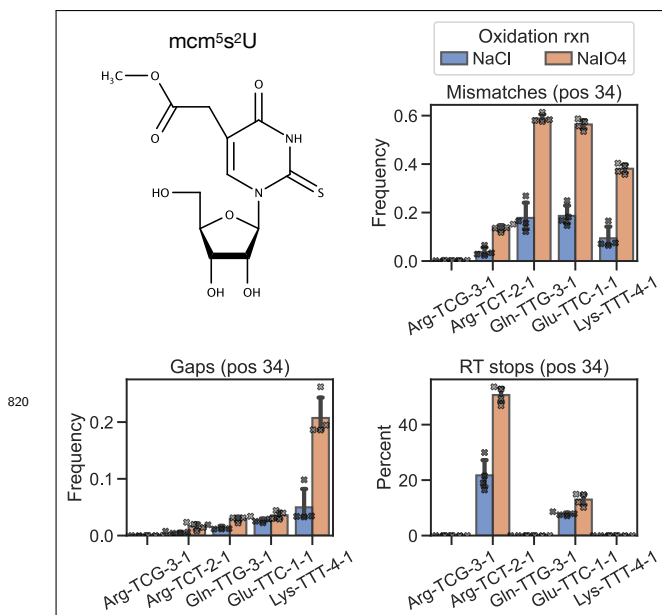


**Figure 3—figure supplement 2.** Mismatch frequency, gap frequency and RT stop percentage is increased upon periodate oxidation for transcripts known to be 5-methoxycarbonylmethyl-2-thiouridine (mcm5s2U) modified. The mcm5s2U modification has been shown to be present on the first anticodon nucleoside (position 34) in human tRNA Lys-UUU, Gln-UUG, Glu-UUC and Arg-UCU, while absent in the similar tRNA Arg-UCG (*Lentini et al., 2018*).

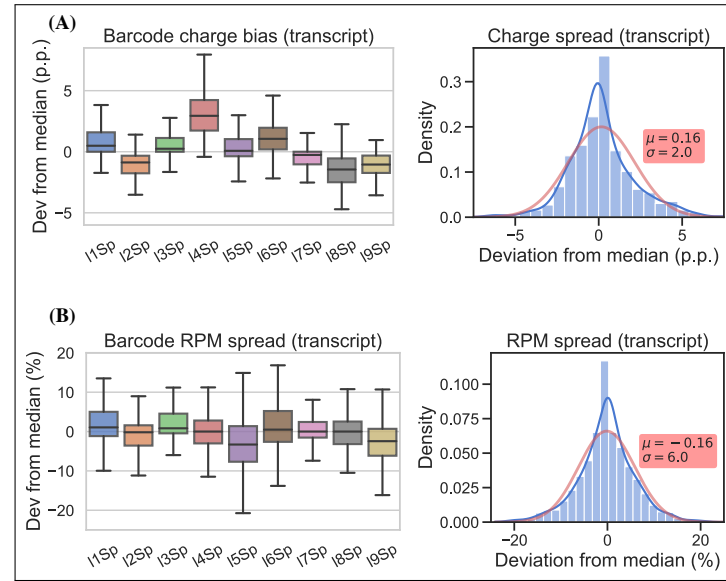


**Figure 4—figure supplement 1.** Similar to **Figure 4**, but at the transcript level.

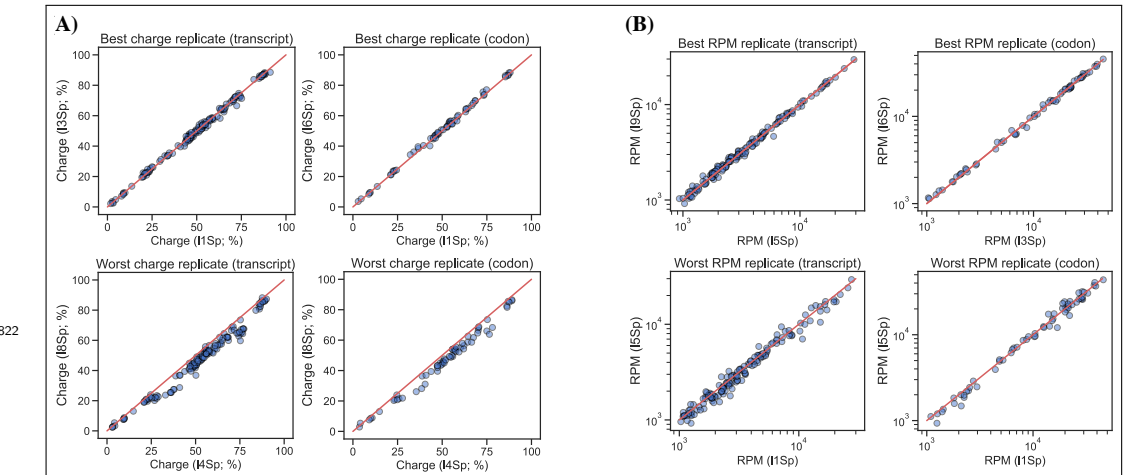


**Figure 4—figure supplement 2.** Best and worst pairwise comparisons between barcode replicates. Sorting pairwise comparisons between barcode replicates according to the sum of squared differences and showing the best and worst either at the transcript or codon level. **(A)** For charge levels, adapter I4Sp tends to overestimate charge. **(B)** For RPM levels. For all plots the red line is proportionality.

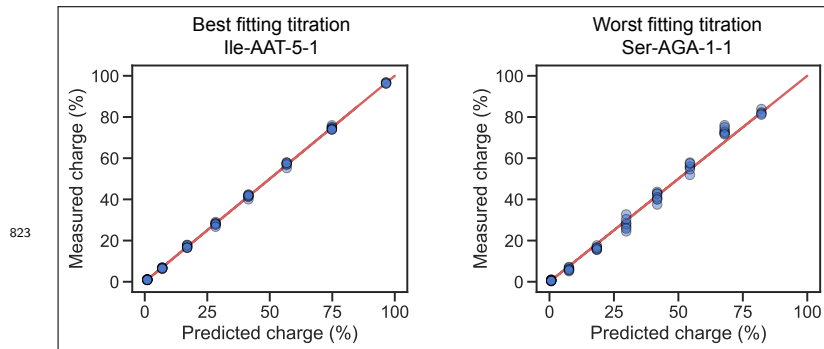


**Figure 5—figure supplement 1.** The best and worst transcript when ranked based on the sum of squared differences between the measured and predicted charge. Related to the representative (i.e. ranked as the median) transcript shown in **Figure 5**, panel B.

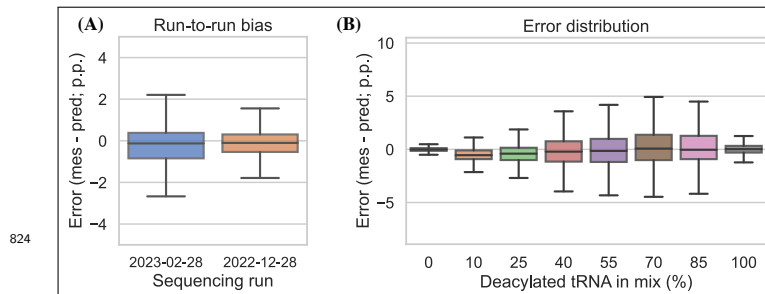


**Figure 5—figure supplement 2.** Charge titration prediction error binned by sequencing run and titration sample. **(A)** Run-to-run bias of two independently prepared sequencing libraries, sequenced on different days. **(B)** Error distribution binned by titration sample. In both panels, error is the percentage point difference between the measured vs. predicted charge for all transcripts in the bin.

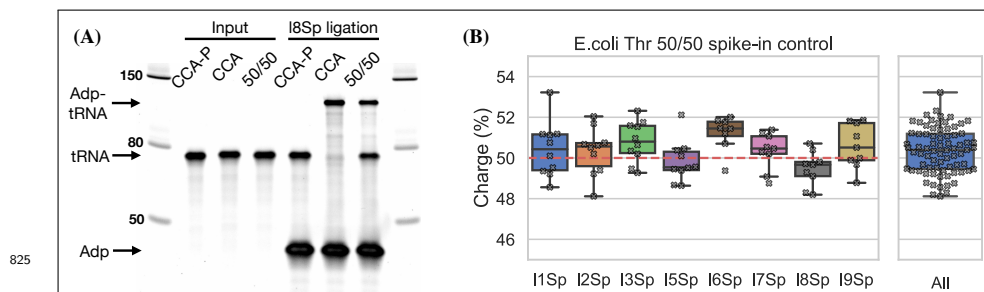


**Figure 5—figure supplement 3.** Spike-in control for 50% charge using the E.coli tRNA-Thr-CGT oligo. **(A)** Ligation between E.coli tRNA-Thr-CCA-Phos and I8Sp is completely blocked indicating ~100% 3' phosphorylation. CCA-P, E.coli tRNA-Thr-CCA-Phos. CCA, E.coli tRNA-Thr-CCA. 50/50, equal mix of CCA-p and CCA. **(B)** E.coli tRNA-Thr spike-in charge measured for samples prepared with an equimolar mix of E.coli tRNA-Thr-CCA-Phos and E.coli tRNA-Thr-CCA. The red dashed line indicates 50% charge.

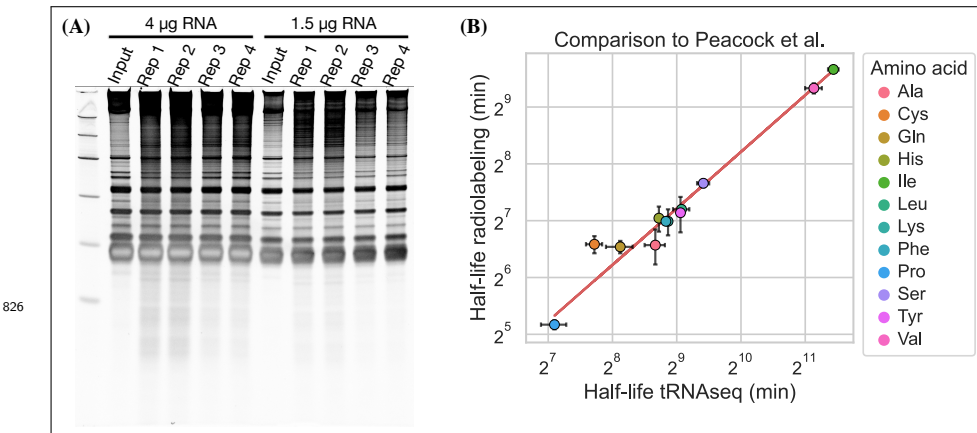


**Figure 6—figure supplement 1.** **(A)** RNA integrity after the last sample was taken (40 h) for the four replicates in the aminoacylation half-life experiment. **(B)** Comparison between aminoacylation half-life estimates grouped by amino acid from this study (tRNAseq) and measurements by *Peacock et al. (2014)* (radiolabeling). Errorbars are +/- standard deviations. A linear regression line is shown as a red line.

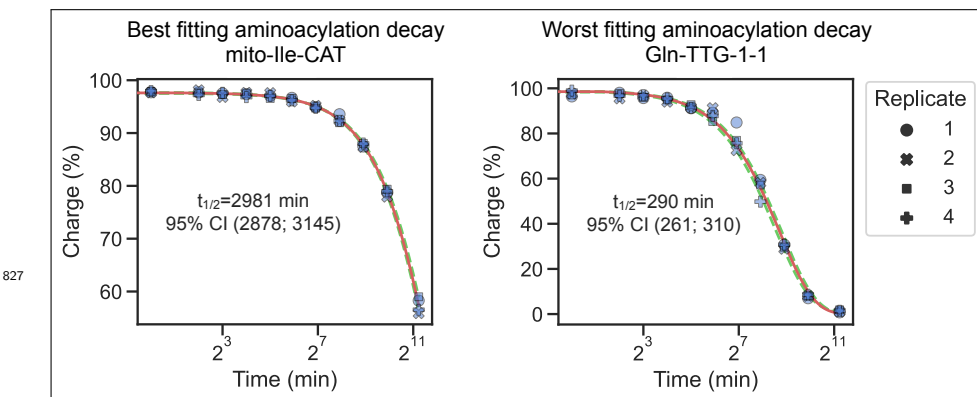


**Figure 6—figure supplement 2.** The best and worst transcript half-life estimates, ranked based on the sum of squared differences between the fitted decay function and the mean charge of the replicates. Related to the representative (i.e. ranked as the median) transcript shown in *Figure 6*, panel A.